

NOAA Technical Memorandum NWS HYDRO-18



NUMERICAL PROPERTIES OF IMPLICIT FOUR-POINT
FINITE DIFFERENCE EQUATIONS OF UNSTEADY FLOW

D. L. Fread

Office of Hydrology
Washington, D.C.
March 1974

noaa

NATIONAL OCEANIC AND
ATMOSPHERIC ADMINISTRATION

National Weather
Service

NOAA TECHNICAL MEMORANDUMS

National Weather Service, Office of Hydrology Series

The Office of Hydrology (HYDRO) of the National Weather Service (NWS) develops procedures for making river and water supply forecasts, analyzes hydrometeorological data for planning and design criteria for other agencies, and conducts pertinent research and development.

NOAA Technical Memorandums in the NWS HYDRO series facilitate prompt distribution of scientific and technical material by staff members, cooperators, and contractors. Information presented in this series may be preliminary in nature and may be published formally elsewhere at a later date. Publication 1 is in the former series, Weather Bureau Technical Notes (TN); publications 2 through 11 are in the former series, ESSA Technical Memorandums, Weather Bureau Technical Memorandums (WBTM). Beginning with 12, publications are now part of the series, NOAA Technical Memorandums, NWS.

Publications listed below are available from the National Technical Information Service, U.S. Department of Commerce, Sills Bldg., 5285 Port Royal Road, Springfield, VA 22161. Prices on request. Order by accession number (given in parentheses). Information on memorandums not listed below can be obtained from Environmental Science Information Center (D822), NOAA, 6009 Executive Boulevard, Rockville, MD 20852.

Weather Bureau Technical Notes

TN 44 HYDRO 1 Infrared Radiation From Air to Underlying Surface. Vance A. Myers, May 1966, 35 pp. (PB-170-664)

ESSA Technical Memorandums

WBTM HYDRO 2 Annotated Bibliography of ESSA Publications of Hydrometeorological Interest. J. L. H. Paulhus, February 1967, 20 pp. (Superseded by WBTM HYDRO 8)

WBTM HYDRO 3 The Role of Persistence, Instability, and Moisture in the Intense Rainstorms in Eastern Colorado, June 14-17, 1965. F. K. Schwarz, February 1967, 21 pp. (PB-174-609)

WBTM HYDRO 4 Elements of River Forecasting. Marshall M. Richards and Joseph A. Strahl, October 1967, 61 pp. (Superseded by WBTM HYDRO 9)

WBTM HYDRO 5 Meteorological Estimation of Extreme Precipitation for Spillway Design Floods. Vance A. Myers, October 1967, 29 pp. (PB-177-687)

WBTM HYDRO 6 Annotated Bibliography of ESSA Publications of Hydrometeorological Interest. J. L. H. Paulhus, November 1967, 27 pp. (Superseded by WBTM HYDRO 8)

WBTM HYDRO 7 Meteorology of Major Storms in Western Colorado and Eastern Utah. Robert L. Weaver, January 1968, 75 pp. (PB-177-491)

WBTM HYDRO 8 Annotated Bibliography of ESSA Publications of Hydrometeorological Interest. J. L. H. Paulhus, August 1968, 25 pp. (Superseded by NWS HYDRO 22)

WBTM HYDRO 9 Elements of River Forecasting (Revised). Marshall M. Richards and Joseph A. Strahl, March 1969, 57 pp. (PB-185-969)

WBTM HYDRO 10 Flood Warning Benefit Evaluation--Susquehanna River Basin (Urban Residences). Harold J. Day, March 1970, 42 pp. (PB-190-984)

WBTM HYDRO 11 Joint Probability Method of Tide Frequency Analysis Applied to Atlantic City and Long Beach Island, N.J. Vance A. Myers, April 1970, 109 pp. (PB-192-745)

NOAA Technical Memorandums

NWS HYDRO 12 Direct Search Optimization in Mathematical Modeling and a Watershed Model Application. John C. Monro, April 1971, 52 pp. (COM-71-00616)

(Continued on inside back cover)

NOAA Technical Memorandum NWS HYDRO-18

NUMERICAL PROPERTIES OF IMPLICIT FOUR-POINT
FINITE DIFFERENCE EQUATIONS OF UNSTEADY FLOW

D. L. Fread

Office of Hydrology
Washington, D.C.
March 1974

Reprinted January 1980

UNITED STATES
DEPARTMENT OF COMMERCE
Juanita M. Kreps, Secretary

NATIONAL OCEANIC AND
ATMOSPHERIC ADMINISTRATION
Richard A. Frank, Administrator

National Weather
Service
Richard E. Halkgren, Director



Preface

This report on the numerical properties of the implicit four-point finite difference equations of unsteady flow is the first in a series of reports which will describe the use of the complete dynamic equations of unsteady flow for computing stages and discharges in rivers, reservoirs, and estuaries. The theory, solution techniques, computer programs, and description of field applications will be presented in forthcoming reports.

ACKNOWLEDGMENTS

The author wishes to express his thanks for the assistance given by Dr. Robert A. Clark and Dr. Eugene L. Peck in reviewing the paper, Mr. Edwin S. Thompson and Mr. Robert Tubella in drafting the figures, and Mrs. Michelle Scott in typing the manuscript.

CONTENTS

Preface	ii
Acknowledgments	ii
List of figures	iv
List of symbols	v
Abstract	1
1. Introduction	1
1.1 Unsteady flow equations	1
1.2 Methods of solution	2
1.3 Implicit four-point difference schemes	3
1.4 Scope of this report	5
2. Stability	6
2.1 Introduction	6
2.2 von Neumann Technique	6
2.3 Numerical experiments	10
3. Convergence	12
3.1 Introduction	12
3.2 Truncation error	12
3.3 Convergence ratios	14
3.4 Mass conservation	23
3.5 Momentum conservation	24
3.6 Numerical experiments	25
4. Summary and conclusions	36
4.1 Summary	36
4.2 Conclusions	37
References	38

S_f	friction slope defined by Eq (52c)
S_b	channel bottom slope
t_o	time
t_o	time of initial rise in the upstream boundary discharge hydrograph when the discharge is steady and equal to Q_o
T	wave period
\tan	tangent trig function
\tan^{-1}	arc tangent trig function
u	solution of differential equation $L(u)$
U	solution of difference approximating equation $L(U)$
v	perturbation velocity
v^*	exact solution of perturbation velocity
V	velocity of flow in cross-section
V_o	mean velocity
V_o^x	velocity of lateral inflow in the x-direction
x^{qx}	distance along the channel as measured in the downstream direction from the upstream boundary
y_j	stage computed with a particular Δt time step
y_p	maximum (peak) value of y_j
Y_s^j	stage computed with a Δt_c^j (explicit time step)
Y_s^p	maximum value of Y_s^j
Y_o	initial depth of flow at time t_o
Z_o	dummy variable equal to $(\lambda-1)$
β	wave parameter equal to $2\pi/T$
γ	skewness parameter of upstream boundary hydrograph defined by Eq (53a)
δh	perturbation error in the depth
δv	perturbation error in the velocity
Δx	computational distance step
Δt	computational time step
Δt_c	computational time step required in explicit methods as determined by the Courant condition, Eq (2)
η	correction factor by which ψ^* is obtained from a given ψ
θ	finite difference weighting factor for spatial derivatives
λ	stability factor defined by Eq (12) and Eq (17a)
π	constant (3.1416...)
ρ	amplification factor of upstream boundary hydrograph defined by Eq (53b)
σ	wave parameter equal to $2\pi/L$
τ	time from beginning of rise to peak of upstream boundary discharge hydrograph
τ_g	time from beginning of rise to center of gravity of upstream boundary discharge hydrograph
ψ	dummy variable representing any particular channel parameter
ψ^*	dummy variable representing any particular channel parameter whose value is different than ψ
∂	partial derivative

LIST OF SYMBOLS

a	coefficient defined by Eq (16a) in stability analysis
A	wetted cross-sectional area
b	coefficient defined by Eq (16b) in stability analysis
B	width of water surface of wetted cross-sectional area
C	wave celerity convergence ratio defined by Eqs (41b and 44b)
C^c	wave damping convergence ratio defined by Eqs (41a and 44a)
D^d	dimensionless Courant parameter defined by Eq (42b)
D^c	dimensionless friction parameter defined by Eq (42c)
D^f	dimensionless parameter of the spatial discretization of the
D^L	wave defined by Eq (42a)
e	base of natural logarithms
E	truncation error
g	acceleration due to gravity
h	perturbation depth
h^*	exact solution of perturbation depth
H	depth of flow
H	mean depth
i^o	complex imaginary unit equal to $\sqrt{-1}$
Im	imaginary component of a complex number
j	counter for number of hydrograph points as used in Eqs (55 and 56)
k	linearized friction parameter defined by Eq(6c)
k^o	counter for number of iterations in Newton-Raphson solution of
	nonlinear system of algebraic equations
K	dummy variable of finite difference expressions of Eqs (4)
ln	natural logarithm
L	wave length
\bar{L}	length of channel reach between upstream and downstream boundaries
m	subscript which identifies spatial location of a variable
M	subscript which identifies the location of the downstream boundary
n	subscript which identifies the time level associated with a
	variable
\bar{n}	Manning roughness coefficient
n^o	total number of hydrograph points associated with Eqs (55 and 56)
O	"order of"
P	wetted perimeter of cross-section
P_e	relative error of the peak stage for a certain set of channel
	parameters
P_e^o	relative error of the peak stage for a different set of channel
	parameters
q	lateral inflow per unit length of channel
Q	maximum discharge at the upstream boundary
Q^{\max}	initial steady discharge at time t_o at the upstream boundary
$Q^o(t)$	discharge at any time t at the upstream boundary
r	coefficient defined by Eq (17a) in stability analysis
R	hydraulic radius equivalent to A/P
Re	real component of a complex number
s	coefficient defined by Eq (17b) in stability analysis
S_e	relative root mean square error of the computed stages for a
	certain set of channel parameters
S_e^o	relative root mean square error of the computed stages for a
	different set of channel parameters

LIST OF FIGURES

<u>Figure No.</u>		<u>Page</u>
1	The x-t Solution Region	4
2a	Damping Convergence Ratio, C_d , Against D_L for Box Scheme with Variations in D_c and $D_f=0.0$	19
2b	Celerity Convergence Ratio, C_c , Against D_L for Box Scheme with Variations in D_c and $D_f=0.0$	19
3a	Damping Convergence Ratio, C_d , Against D_L for Box Scheme with Variations in D_c and $D_f=0.4$	20
3b	Celerity Convergence Ratio, C_c , Against D_L for Box Scheme with Variations in D_c and $D_f=0.4$	20
4a	Damping Convergence Ratio, C_d , Against D_L for Box Scheme with Variations in D_c and $D_f=1.0$	21
4b	Celerity Convergence Ratio, C_c , Against D_L for Box Scheme with Variations in D_c and $D_f=1.0$	21
5a	Damping Convergence Ratio, C_d , Against D_L for Backward Implicit Scheme with Variations in D_c and $D_f=0.0$	22
5b	Celerity Convergence Ratio, C_c , Against D_L for Backward Implicit Scheme with Variations in D_c and $D_f=0.0$	22
6	Distortion of Computed Downstream Stage Hydrograph for Large Δt Steps When θ is Varied and $\tau=48$ Hours	29
7	Distortion of Computed Downstream Stage Hydrograph for Large Δt Steps When θ is Varied and $\tau=120$ Hours	30
8	Effect of θ and τ on the Distortion of the Computed Stage Hydrograph at the Downstream Boundary for Various Δt Time Steps Having $\rho=20$ and $\gamma=1.2$	31
9	Correlation of S_e Error (for the Stage at the Downstream Boundary) with the Δt Time Step for Various Upstream Boundary Hydrographs Having $\gamma=1.2$	32
10	Correlation of P_e Error (for the Stage at the Downstream Boundary) with the Δt Time Step for Various Upstream Boundary Hydrographs Having $\gamma=1.2$	34
11	Correction Factor, η , for Determining the Effect of Various Channel Parameters on the Numerical Distortion (S_e, P_e)	35

NUMERICAL PROPERTIES OF
IMPLICIT FOUR-POINT FINITE DIFFERENCE EQUATIONS OF UNSTEADY FLOW

Abstract

Linearized model equations of the quasi-linear differential equations of unsteady gradually varied flow are utilized to investigate the effect of the discretization of the continuous partial derivatives with implicit four-point finite difference quotients. Through use of a weighting factor (θ) which positions the spatial difference quotient between adjacent time levels in the x-t solution region, the investigation is generalized to include the various four-point implicit difference schemes that have been reported in the literature.

Numerical stability properties of the four-point difference schemes are analyzed via the von Neumann method. When $0.5 \leq \theta \leq 1.0$, the difference equations are found to be unconditionally linearly stable and conditionally stable when $\theta < 0.5$.

The convergence properties are qualitatively investigated by determining the truncation error. The backward implicit scheme ($\theta=1.0$) has a first order truncation error, i.e., $E=O(\Delta t)+O(\Delta x^2)$; whereas, the box implicit scheme ($\theta=0.5$) has a second order truncation error, i.e., $E=O(\Delta t^2)+O(\Delta x^2)$.

The convergence properties are quantitatively investigated by determining analytical expressions for wave damping and wave celerity convergence ratios, e.g., numerical damping/physical wave damping. These expressions are nondimensionalized in terms of convenient dimensionless parameters, and graphs are presented which quantify the convergence ratios for a wide range of the dimensionless parameters. The box scheme is shown to possess superior convergence properties compared to the backward implicit scheme, particularly with respect to wave damping. On the basis of convergence properties, the box scheme is shown to be the preferred implicit four-point difference scheme for discretizing the differential equations of unsteady flow.

1. INTRODUCTION

1.1 Unsteady Flow Equations

The motion of a long wave in a river or estuary such as a flood wave, tide, or storm surge is usually considered one-dimensional, i.e., the accelerations and velocity components of the wave in the transverse and vertical directions are not considered. Hence, the motion of the wave is described solely in the direction of the longitudinal axis of the river by the one-dimensional differential equations of unsteady gradually varied flow. The equations consist of: (1) the continuity equation which conserves the mass of the wave,

$$\frac{\partial A}{\partial t} + \frac{\partial (AV)}{\partial x} - q = 0 \tag{1a}$$

and (2) the equation of motion or dynamic equilibrium which conserves the momentum of the wave,

$$\frac{\partial V}{\partial t} + \frac{1}{2} \frac{\partial V^2}{\partial x} + g \left(\frac{\partial H}{\partial x} - S_o + \frac{\bar{n}^2 |V| V}{2.21 R^{4/3}} \right) + (V - V_{qx}) \frac{q}{A} = 0 \quad (1b)$$

in which x = the distance along the river axis, positive in the downstream direction; t = time; A = wetted cross-sectional area; V = mean velocity in a cross section; H = depth of flow in a cross section; S_o = channel bottom slope; q = lateral inflow per unit length along the river axis; V_{qx} = mean velocity of lateral inflow in the x -direction; R = the hydraulic radius; \bar{n} = Manning's roughness coefficient; and g = acceleration due to gravity.

Eqs. (1) are quasi-linear, first order, first degree partial differential equations of the hyperbolic type. They have two independent variables, x and t , and two dependent variables, H and V . The other terms are either known functions of x , t , H , and/or V , or they are constants. No analytical solutions to this system of equations are presently known except for cases where channel geometry is uncomplicated and the nonlinear properties of the equations are either neglected or made linear. However, Eqs. (1) can be approximated by finite differences, and the resulting difference equations numerically integrated via high speed digital computers to obtain solutions of H and V for discrete values of x and t .

1.2 Methods of Solution

Numerous finite difference techniques have been developed to solve Eqs. (1). These techniques can be classified into three categories:

- (1) Finite differences of the transformed forms of Eqs. (1), called characteristic equations, using either a fixed grid, e.g., Lister [1960], Baltzer and Lai [1968], Yevjevich and Barnes [1970]; or a characteristic grid, e.g., Lister [1960], Amein [1966], and Liggett and Woolhiser [1967];
- (2) Explicit finite difference schemes, e.g., Stoker [1956, 1957], Dronkers [1969], and Garrison et al. [1969]; and
- (3) Implicit finite difference schemes, e.g., Abbott and Ionescu [1967], Lai [1967], Baltzer and Lai [1968], Dronkers [1969], Amein and Fang [1970], Gunaratnam and Perkins [1970], Contractor and Wiggert [1971], and Fread [1973b].

The characteristic and explicit schemes are relatively simple compared to the implicit schemes; however, they are restricted in the size of the computational time step required to achieve a stable computational procedure. Numerical stability is the condition wherein small numerical errors do not increase in magnitude with succeeding computations such that the true solution is masked by the errors. The restriction in Δt is manifested by the following inequality, known as the Courant stability criterion [Stoker,

1957; Strelkoff, 1970]:

$$\Delta t \leq \left[\frac{\Delta x_m}{V_m + \sqrt{gA_m/B_m}} \right] \text{ minimum for all } m \text{ points} \quad (2)$$

where B is the width of the water surface in the m^{th} cross-section, Δx_m is the m^{th} finite difference distance interval, and Δt is the computational time step. Frictional considerations may further limit the maximum allowable Δt as manifested by the following stability criterion [Garrison et al., 1969]:

$$\Delta t \leq \left[\left(\frac{\Delta x_m}{V_m + \sqrt{gA_m/B_m}} \right) \left(1 - \frac{gn^{-2} |V_m| \Delta t}{2.21 R_m^{4/3}} \right) \right] \text{ minimum for all } m \text{ points} \quad (3)$$

Inspection of the above stability criteria indicates that the computational time step is substantially reduced as the hydraulic depth (A/B) increases. Thus, in deep rivers, it is not uncommon for time steps on the order of minutes or even seconds to be required even though the flood wave may be very gradual having a duration in the order of weeks. Such small time steps cause the explicit and characteristic difference schemes to be very inefficient in the use of computer time.

Another requirement of explicit and characteristic schemes is the use of equal distance intervals. This restriction is disadvantageous for rivers with irregular geometry.

In order to negate the restriction of small time steps imposed on the explicit and characteristic schemes for reasons of stability, implicit difference schemes were developed. Several of the implicit difference schemes have been shown to be computationally stable and independent of the size of the time and distance steps. Abbott and Ionescu [1966], Leendertse [1966], Dronkers [1969], Gunaratnam and Perkins [1970], and Strelkoff [1971] presented analytical stability analyses of various implicit schemes while others have demonstrated the stability of implicit schemes via numerical experiments, e.g., Amein and Fang [1970] and Fread [1973a]. Also, analytical analyses of the accuracy or convergence properties of some implicit schemes have been presented, viz., Leendertse [1966], and Gunaratnam and Perkins [1970].

1.3 Implicit Four-Point Difference Schemes

Of the various implicit schemes which have been developed, the "four-point" schemes appear most advantageous since they can readily be used with unequal distance intervals. These schemes have been used by Baltzer and Lai [1968], Amein and Fang [1970], Contractor and Wiggert [1971], and Fread [1973a]. A description of the implicit four-point difference schemes follows.

The continuous x - t region in which solutions of H and V are sought may be represented by a rectangular net of discrete points as shown in Fig. 1.

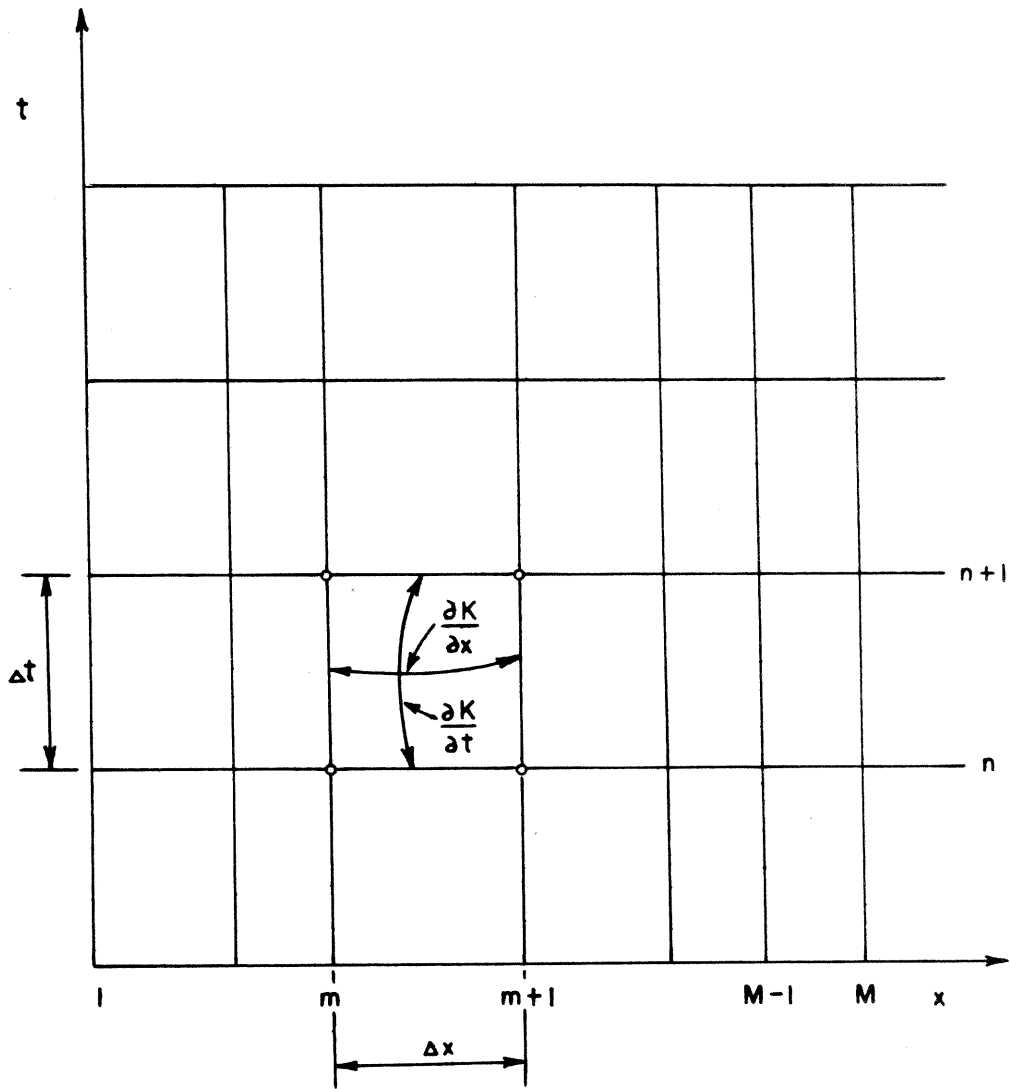


Fig. 1- The $x-t$ Solution Region.

The net points are seen to be defined by the intersection of straight lines drawn parallel to the axes of the x-t region. Lines parallel to the x-axis are time lines and have a spacing of Δt which need not be constant. Lines parallel to the t-axis represent discrete locations along the river and have a spacing of Δx which need not be constant. Each discrete point is identified by a subscript which designates the x-position and a superscript which designates the time line.

In implicit four-point difference schemes, the time derivatives are approximated by a forward difference operator centered between the m^{th} and $m+1$ points along the x-axis, i.e.,

$$\frac{\partial K}{\partial t} \approx \frac{K_m^{n+1} + K_{m+1}^{n+1} - K_m^n - K_{m+1}^n}{2\Delta t} \quad (4a)$$

where K represents any variable. The spatial derivatives are approximated by a forward difference operator positioned between two adjacent time lines according to weighting factors of θ and $1-\theta$, i.e.,

$$\frac{\partial K}{\partial x} \approx \theta \left(\frac{K_{m+1}^{n+1} - K_m^{n+1}}{\Delta x} \right) + (1-\theta) \left(\frac{K_{m+1}^n - K_m^n}{\Delta x} \right) \quad (4b)$$

Variables or functions other than derivatives are approximated at the time level where the spatial derivative is evaluated by using weighting factors similar to those of Eq. (4b). Thus,

$$K \approx \theta \left(\frac{K_m^{n+1} + K_{m+1}^{n+1}}{2} \right) + (1-\theta) \left(\frac{K_m^n + K_{m+1}^n}{2} \right) \quad (4c)$$

A θ weighting factor of unity yields the backward implicit scheme used by Baltzer and Lai [1968] and Dronkers [1969]. A θ weighting factor of 0.5 yields the "box" scheme used by Amein and Fang [1970], Contractor and Wiggert [1971], and Fread [1973b]. The four-point difference scheme becomes implicit for all values of θ greater than zero.

1.4 Scope of this Report

Although the implicit four-point difference equations have received attention in the literature, a detailed numerical analysis of the schemes has been lacking although some numerical experiments were reported by Amein and Fang [1970] and Fread [1973a]. It is the purpose of this report to present a detailed analysis of the numerical properties (stability and convergence) of the implicit four-point difference schemes when applied to the unsteady flow equations. Both analytical analyses and numerical simulation techniques will be utilized to study their stability and convergence properties.

2. STABILITY

2.1 Introduction

It is essential that the discrete steps of time and distance in the integration of the finite difference equations provide a solution which is bounded. Such a solution is numerically stable, i.e., the numerical errors introduced in the computations through round-off are not amplified during successive computations such as to entirely mask the true solution.

2.2 von Neumann Technique

An analytical technique for investigating numerical stability was developed by von Neumann and presented in detail by O'Brien et al. [1951]. The von Neumann technique is used herein to investigate the stability properties of the four-point implicit schemes. Since it is only applicable to linear differential equations, it is necessary to linearize Eqs. (1). The linearized equations are then simplified by omitting certain terms on the basis of their relatively small magnitude in order to facilitate the stability analysis. Hence, the equations which will be analyzed represent a model of the original nonlinear differential equations; nonetheless, considerable understanding of the numerical properties of nonlinear equations can be attained from this kind of analysis.

The model equations are applicable to a broad channel with no lateral inflow; hence, $R=H$ and $q=0$. The linearization of Eqs. (1) is accomplished by substituting a small perturbation in depth h above a mean depth H_0 and velocity v above a mean velocity V_0 , i.e.,

$$H = H_0 + h \quad (5a)$$

$$V = V_0 + v \quad (5b)$$

Upon performing the above mentioned substitutions and simplifications, the following model equations are obtained:

$$\frac{\partial h}{\partial t} + H_0 \frac{\partial v}{\partial x} = 0 \quad (6a)$$

$$\frac{\partial v}{\partial t} + g \frac{\partial h}{\partial x} + kv = 0 \quad (6b)$$

where

$$k = \frac{g V_0 \bar{n}^2}{1.1 H_0^{4/3}} \quad (6c)$$

Eqs. (6) are the same as investigated by Leendertse [1966] and Dronkers [1969].

The four-point implicit difference approximations to the model equations are obtained by substituting the finite difference expressions given by Eqs. (4) into Eqs. (6). Thus,

$$\frac{h_m^{n+1} + h_{m+1}^{n+1} - h_m^n - h_{m+1}^n}{2\Delta t} + \theta H_0 \left(\frac{v_{m+1}^{n+1} - v_m^{n+1}}{\Delta x} \right) + (1-\theta) H_0 \left(\frac{v_{m+1}^n - v_m^n}{\Delta x} \right) = 0 \quad (7a)$$

$$\begin{aligned} & \frac{v_m^{n+1} + v_{m+1}^{n+1} - v_m^n - v_{m+1}^n}{2\Delta t} + \theta \left[g \frac{(h_{m+1}^{n+1} - h_m^{n+1})}{\Delta x} + k \left(\frac{v_m^{n+1} + v_{m+1}^{n+1}}{2} \right) \right] \\ & + (1-\theta) \left[g \left(\frac{h_{m+1}^n - h_m^n}{\Delta x} \right) + k \left(\frac{v_m^n + v_{m+1}^n}{2} \right) \right] = 0 \end{aligned} \quad (7b)$$

Eqs. (7) are investigated for their stability properties by the von Neumann technique in which a Fourier expansion of a line of errors is followed as time progresses. The Fourier series can be formulated in terms of sines and cosines; however, the algebra is easier if the complex exponential form is used. To further ease the analysis, only one term of the Fourier series need be considered since Eqs. (7) represent a linear system. The errors are given by the following truncated series:

$$\delta h(x, t) = h^* e^{i(\sigma x + \beta t)} \quad (8a)$$

$$\delta v(x, t) = v^* e^{i(\sigma x + \beta t)} \quad (8b)$$

Where δh and δv are the errors in the depth and velocity, respectively; h^* and v^* are the exact solutions of the depth and velocity in the difference equations; i is the complex imaginary unit equal to $\sqrt{-1}$; $\beta = 2\pi/T$, where T is the period of the wave or the time it takes for the complete wave to pass a fixed point; and $\sigma = 2\pi/L$, where L is the wave length which is given by the product of the wave period and the propagation speed of the wave. Since

$$x = m \Delta x \quad (9a)$$

$$t = n \Delta t \quad (9b)$$

the errors can be expressed at discrete points in the x - t solution region, viz.,

$$\delta h_m^n = h^* e^{i(\sigma m \Delta x + \beta n \Delta t)} \quad (10a)$$

$$\delta h_{m+1}^{n+1} = h^* e^{i[\sigma(m+1)\Delta x + \beta(n+1)\Delta t]} \quad (10b)$$

The errors are assumed to be perturbations imposed on the solution of the linear system. If the exact difference equations are subtracted from the difference equations which include the errors, equations are formed which are quite similar to Eqs. (7) but in terms of the errors. If these error equations are then divided by $e^{i\sigma\Delta x} e^{i\beta n\Delta t}$, the following error expressions are obtained:

$$h^* [\lambda (e^{i\sigma\Delta x} + 1) - (e^{i\sigma\Delta x} - 1)] + v^* [H \frac{\Delta t}{\Delta x} (2\theta\lambda + 2 - 2\theta) (e^{i\sigma\Delta x} - 1)] = 0 \quad (11a)$$

$$h^* [g \frac{\Delta t}{\Delta x} (2\theta\lambda + 2 - 2\theta) (e^{i\sigma\Delta x} - 1)] + v^* (e^{i\sigma\Delta x} + 1) [\lambda - 1 + k\Delta t (\theta\lambda + 1 - \theta)] = 0 \quad (11b)$$

where

$$\lambda = e^{i\beta\Delta t} \quad (12)$$

Upon dividing Eqs. (11) by $(e^{i\sigma\Delta x} + 1)$ and substitution of the complex identity,

$$i \tan(\sigma\Delta x/2) = \frac{(e^{i\sigma\Delta x} - 1)}{(e^{i\sigma\Delta x} + 1)} \quad (13)$$

the following equations are obtained:

$$(\lambda - 1)h^* + [(2\theta\lambda + 2 - 2\theta)H \frac{\Delta t}{\Delta x} i \tan(\sigma\Delta x/2)]v^* = 0 \quad (14a)$$

$$[(2\theta\lambda + 2 - 2\theta)g \frac{\Delta t}{\Delta x} i \tan(\sigma\Delta x/2)]h^* + [\lambda - 1 + k\Delta t (\theta\lambda + 1 - \theta)]v^* = 0 \quad (14b)$$

In order for the difference equations, Eqs. (7), to be stable, it is necessary that the error at time $t + \Delta t$ be smaller than the error at time t . Consequently, $|\lambda| = |e^{i\beta\Delta t}|$, as defined in Eq. (12), must be smaller than or equal to unity. A relation may be found between λ , σ , and the coefficients of the difference equations containing Δx and Δt . The von Neumann stability criterion, which must hold for all possible σ , then determines the final relation between λ and the coefficients. Stability in the sense of von Neumann is based on the conjecture that linear operators with variable coefficients are stable if and only if all their localized operators, in which coefficients are taken as constant, are stable. Thus, in the von Neumann technique, when it is found that $|\lambda| < 1$ is independent of the values of Δx and Δt , the difference equations are unconditionally linearly stable; however, if $|\lambda| < 1$ for only certain intervals of $\Delta t/\Delta x$, the equations are conditionally stable. When $|\lambda| = 1$, the difference equations are neutrally

or weakly stable; and when $|\lambda| > 1$, the equations are unconditionally linearly unstable.

A relationship between λ , σ , and the coefficients of the error equations can be obtained by eliminating v^* from Eqs. (14) and then dividing by h^* . Thus, the following expression is obtained:

$$(\lambda-1) [\lambda-1+\theta(\lambda-1)b+b] + 4[\theta(\lambda-1)+1]^2 a = 0 \quad (15)$$

where

$$a = g H_0 \left(\frac{\Delta t}{\Delta x} \right)^2 \tan^2(\sigma \Delta x / 2) \quad (16a)$$

$$b = k \Delta t \quad (16b)$$

Eq. (15) may be solved for λ by using the substitution, $z=\lambda-1$. In this way, the following expression for λ is obtained:

$$\lambda = r + is \quad (17a)$$

where

$$r = 1 - \frac{(8\theta a + b)}{2(1 + 4\theta^2 a + \theta b)} \quad (17b)$$

$$s = \frac{\sqrt{16a - b^2}}{2(1 + 4\theta^2 a + \theta b)} \quad (17c)$$

From Eqs. (17), an expression for $|\lambda|$ may be obtained. Thus,

$$|\lambda| = \sqrt{r^2 + s^2} = \sqrt{\frac{1 + (2\theta - 2)^2 a + (\theta - 1)b}{1 + 4\theta^2 a + \theta b}} \quad (18)$$

Eq. (18) may be used to determine the stability of various implicit four-point difference equations by substituting different values of θ and examining the resulting expression to see if it is less than, equal to, or greater than unity.

When θ is unity,

$$|\lambda| = \sqrt{\frac{1}{1 + 4a + b}} \quad (19)$$

Therefore, $|\lambda| \leq 1$ and the backward implicit four-point difference scheme is unconditionally linearly stable.

When θ is 0.5,

$$|\lambda| = \sqrt{\frac{1+a-b/2}{1+a+b/2}} \quad (20)$$

Therefore, $|\lambda| \leq 1$ and the box or centered four-point difference scheme is unconditionally linearly stable.

When θ assumes values in the range $0 < \theta < 0.5$ in Eq. (18), it is seen that the condition whereby $|\lambda| \leq 1$ is not independent of the values of a and b ; therefore, since a and b are functions of Δx and Δt , the four-point implicit difference equations are conditionally linearly stable for θ values less than 0.5.

When frictional effects are negligible, k as defined by Eq. (6c) tends to zero as does b which is given by Eq. (16b). For this condition, the fully implicit scheme remains unconditionally stable; however, the box scheme becomes neutrally or weakly stable. Under some conditions, the neutrally stable box scheme will exhibit a tendency for the numerical solution to oscillate about the true solution. Since the oscillations are bounded and are not large relative to the solution, this condition is one of pseudo-instability which is sometimes referred to as a computational mode. Some investigators have apparently mistaken this condition for a serious instability and have chosen the backward implicit scheme in order to avoid the computational mode. If the pseudo-instability of the neutrally stable box scheme proves to be an inconvenience, it has been observed via numerical experiments that it may be essentially eliminated by using a θ of approximately 0.55. This is recommended for reasons of accuracy, as will be shown later, rather than using the backward implicit scheme.

In the preceding analysis, a simple model system of the original complex nonlinear system was investigated. The model was locally linearized and given constant coefficients. The influence of boundary conditions, i.e., the amplitude and shape of the wave, was not considered. It is hoped then that a finite difference scheme which is stable for the model system will remain stable for the more complex nonlinear system. Computing experience has shown that the heuristic analysis provided by the von Neumann technique will usually provide a true description of the stability properties of finite difference schemes for nonlinear systems; however, it does not insure that a stable scheme will always be stable. Nevertheless, those schemes are identified which are fundamentally unstable.

2.3 Numerical Experiments

Stability may be investigated via numerical experiments in which the difference equations of the nonlinear system are tested with different time and distance steps for various wave conditions. Although this type of

analysis can deal directly with the complex nonlinear system, it is limited in that it is difficult and sometimes misleading to extend the results beyond the range of computational intervals and wave conditions which are tested. The numerical experiments reported by Fread [1973a] tend to agree with the results of the stability analysis presented herein; however, it is noted that in the numerical experiments, the implicit four-point scheme with θ values in the range of 0.5 did exhibit instabilities when the time steps were quite large relative to the wave period, i.e., $\Delta t \approx T/4$, and when the wave condition approached that of an abrupt rather than gradual wave. The four-point scheme was found to become stable for such severe conditions if θ was increased such that the difference scheme approached the backward implicit scheme, but at the expense of a loss in accuracy. This property of the four-point schemes is discussed in the next section.

3. CONVERGENCE

3.1 Introduction

Convergence is the condition in which the solution of the finite difference equation for a finite grid size approaches the analytical solution of the partial differential equation. This means that if u is the solution of the differential equation $L(u)$, and if U is the solution of the difference approximating equation $[L(u)]^{n+1/2}$ which is in discrete form, then the conditions under which the convergence ratio U/u approaches unity are the convergence conditions.

3.2 Truncation Error

Convergence may be investigated qualitatively by determining the functional form of the truncation or discretization error. This error is the difference between the solution of the difference equation and that of the partial differential equation. The solution of the difference equation is found by expanding each term in a Taylor Series expansion about the point at which the differential equation is computed. In this case, the point is the center of the grid shown in Fig. 1, i.e., the point $(m+1/2, n+1/2)$.

First, expanding K_m^n and K_m^{n+1} about the point $(m, n+1/2)$ gives the following:

$$(K_m^n)^{n+1/2} = K_m^{n+1/2} - \frac{\Delta t}{2} \left(\frac{\partial K}{\partial t} \right)_m^{n+1/2} + \frac{\Delta t^2}{8} \left(\frac{\partial^2 K}{\partial t^2} \right)_m^{n+1/2} - \frac{\Delta t^3}{48} \left(\frac{\partial^3 K}{\partial t^3} \right)_m^{n+1/2} + \dots \quad (21a)$$

$$(K_m^{n+1})^{n+1/2} = K_m^{n+1/2} + \frac{\Delta t}{2} \left(\frac{\partial K}{\partial t} \right)_m^{n+1/2} + \frac{\Delta t^2}{8} \left(\frac{\partial^2 K}{\partial t^2} \right)_m^{n+1/2} + \frac{\Delta t^3}{48} \left(\frac{\partial^3 K}{\partial t^3} \right)_m^{n+1/2} + \dots \quad (21b)$$

Therefore,

$$\left(\frac{K_m^{n+1} - K_m^n}{\Delta t} \right)_m^{n+1/2} = \left(\frac{\partial K}{\partial t} \right)_m^{n+1/2} + \frac{\Delta t^2}{24} \left(\frac{\partial^3 K}{\partial t^3} \right)_m^{n+1/2} + \dots \quad (22a)$$

In a similar manner,

$$\left(\frac{K_{m+1}^{n+1} - K_{m+1}^n}{\Delta t} \right)_{m+1}^{n+1/2} = \left(\frac{\partial K}{\partial t} \right)_{m+1}^{n+1/2} + \frac{\Delta t^2}{24} \left(\frac{\partial^3 K}{\partial t^3} \right)_{m+1}^{n+1/2} + \dots \quad (22b)$$

Now, expanding Eqs. (22) about the center point $(m+1/2, n+1/2)$ gives:

$$\begin{aligned} \left(\frac{K_m^{n+1} - K_m^n}{\Delta t} \right)_{m+1/2}^{n+1/2} &= \left(\frac{\partial K}{\partial t} \right)_{m+1/2}^{n+1/2} + \frac{\Delta t^2}{24} \left(\frac{\partial^3 K}{\partial t^3} \right)_{m+1/2}^{n+1/2} - \frac{\Delta x}{2} \left[\left(\frac{\partial^2 K}{\partial x \partial t} \right)_{m+1/2}^{n+1/2} \right. \\ &+ \frac{\Delta t^2}{24} \left(\frac{\partial^4 K}{\partial x \partial t^3} \right)_{m+1/2}^{n+1/2} + \dots \left. + \frac{\Delta x^2}{8} \left[\left(\frac{\partial^3 K}{\partial x^2 \partial t} \right)_{m+1/2}^{n+1/2} + \frac{\Delta t^2}{24} \left(\frac{\partial^5 K}{\partial x^2 \partial t^3} \right)_{m+1/2}^{n+1/2} + \dots \right] - \dots \quad (23a) \end{aligned}$$

$$\begin{aligned}
\left(\frac{K^{n+1}-K^n}{\Delta t}\right)_{m+1/2}^{n+1/2} &= \left(\frac{\partial K}{\partial t}\right)_{m+1/2}^{n+1/2} + \frac{\Delta t^2}{24} \left(\frac{\partial^3 K}{\partial t^3}\right)_{m+1/2}^{n+1/2} + \frac{\Delta x}{2} \left[\left(\frac{\partial^2 K}{\partial x \partial t}\right)_{m+1/2}^{n+1/2}\right. \\
&+ \frac{\Delta t^2}{24} \left(\frac{\partial^4 K}{\partial x \partial t^3}\right)_{m+1/2}^{n+1/2} + \dots \left. + \frac{\Delta x^2}{8} \left[\left(\frac{\partial^3 K}{\partial x^2 \partial t}\right)_{m+1/2}^{n+1/2} + \frac{\Delta t^2}{24} \left(\frac{\partial^5 K}{\partial x^2 \partial t^3}\right)_{m+1/2}^{n+1/2} + \dots\right] + \dots \quad (23b)
\end{aligned}$$

In a manner similar to that used in Eqs. (21, 22, and 23), the following expansions are obtained:

$$\begin{aligned}
\left(\frac{K^{n+1}-K^n}{\Delta x}\right)_{m+1/2}^{n+1/2} &= \left(\frac{\partial K}{\partial x}\right)_{m+1/2}^{n+1/2} + \frac{\Delta x^2}{24} \left(\frac{\partial^3 K}{\partial x^3}\right)_{m+1/2}^{n+1/2} - \frac{\Delta t}{2} \left[\left(\frac{\partial^2 K}{\partial t \partial x}\right)_{m+1/2}^{n+1/2}\right. \\
&+ \frac{\Delta x^2}{24} \left(\frac{\partial^4 K}{\partial t \partial x^3}\right)_{m+1/2}^{n+1/2} + \dots \left. + \frac{\Delta t^2}{8} \left[\left(\frac{\partial^3 K}{\partial t^2 \partial x}\right)_{m+1/2}^{n+1/2} + \frac{\Delta x^2}{24} \left(\frac{\partial^5 K}{\partial t^2 \partial x^3}\right)_{m+1/2}^{n+1/2} + \dots\right] - \dots \quad (24a)
\end{aligned}$$

$$\begin{aligned}
\left(\frac{K^{n+1}-K^{n+1}}{\Delta x}\right)_{m+1/2}^{n+1/2} &= \left(\frac{\partial K}{\partial x}\right)_{m+1/2}^{n+1/2} + \frac{\Delta x^2}{24} \left(\frac{\partial^3 K}{\partial x^3}\right)_{m+1/2}^{n+1/2} + \frac{\Delta t}{2} \left[\left(\frac{\partial^2 K}{\partial t \partial x}\right)_{m+1/2}^{n+1/2}\right. \\
&+ \frac{\Delta x^2}{24} \left(\frac{\partial^4 K}{\partial t \partial x^3}\right)_{m+1/2}^{n+1/2} + \dots \left. + \frac{\Delta t^2}{8} \left[\left(\frac{\partial^3 K}{\partial t^2 \partial x}\right)_{m+1/2}^{n+1/2} + \frac{\Delta x^2}{24} \left(\frac{\partial^5 K}{\partial t^2 \partial x^3}\right)_{m+1/2}^{n+1/2} + \dots\right] + \dots \quad (24b)
\end{aligned}$$

Since in Eqs. (23 and 24) all derivatives are expressed at the center point $(m+1/2, n+1/2)$, this notation will henceforth not be used. Eqs. (4) may now be expressed in terms of their Taylor Series expansion about the point $(m+1/2, n+1/2)$ by substituting the expressions given in Eqs. (23 and 24) for the same terms in Eqs. (4). Thus,

$$\frac{\partial K}{\partial t} \approx \frac{K_m^{n+1} + K_{m+1}^{n+1} - K_m^n - K_{m+1}^n}{2\Delta t} = \frac{\partial K}{\partial t} + \frac{\Delta t^2}{24} \frac{\partial^3 K}{\partial t^3} + \frac{\Delta x^2}{8} \left(\frac{\partial^3 K}{\partial x^2 \partial t} + \frac{\Delta t^2}{8} \frac{\partial^5 K}{\partial x^2 \partial t^3}\right) + \dots \quad (25a)$$

$$\begin{aligned}
\frac{\partial K}{\partial x} &\approx \theta \left(\frac{K_{m+1}^{n+1} - K_m^{n+1}}{\Delta x}\right) + (1-\theta) \left(\frac{K_m^n - K_{m+1}^n}{\Delta x}\right) = \frac{\partial K}{\partial x} + (2\theta-1) \frac{\Delta t}{2} \left(\frac{\partial^2 K}{\partial t \partial x} + \frac{\Delta x^2}{24} \frac{\partial^4 K}{\partial t \partial x^3}\right) \\
&+ \frac{\Delta t^2}{8} \left(\frac{\partial^3 K}{\partial t^2 \partial x} + \frac{\Delta x^2}{24} \frac{\partial^5 K}{\partial t^2 \partial x^3}\right) + \frac{\Delta x^2}{24} \frac{\partial^3 K}{\partial x^3} + \dots \quad (25b)
\end{aligned}$$

Through use of the general expressions developed above, the following Taylor series expansion for Eq. (7a) may be obtained:

$$\begin{aligned}
\frac{\partial h}{\partial t} + \frac{\Delta t^2}{24} \frac{\partial^3 h}{\partial t^3} + \frac{\Delta x^2}{8} \left(\frac{\partial^3 h}{\partial x^2 \partial t} + \frac{\Delta t^2}{24} \frac{\partial^5 h}{\partial x^2 \partial t^3}\right) + H_0 \left[\frac{\partial v}{\partial x} + (2\theta-1) \frac{\Delta t}{2} \left(\frac{\partial^2 v}{\partial t \partial x}\right)\right. \\
\left. + \frac{\Delta x^2}{24} \frac{\partial^4 v}{\partial t \partial x^3}\right] + \frac{\Delta t^2}{8} \left(\frac{\partial^3 v}{\partial t^2 \partial x} + \frac{\Delta x^2}{24} \frac{\partial^5 v}{\partial t^2 \partial x^3}\right) + \frac{\Delta x^2}{24} \frac{\partial^3 v}{\partial x^3} + \dots = 0 \quad (26)
\end{aligned}$$

The truncation error (E) can be determined by subtracting Eq. (6a) from Eq. (26). Thus,

$$\begin{aligned}
 E = & (2\theta-1) \frac{\Delta t}{2} H_0 \left(\frac{\partial^2 v}{\partial t \partial x} + \frac{\Delta x^2}{24} \frac{\partial^4 v}{\partial t \partial x^3} \right) + H_0 \frac{\Delta t^2}{8} \left(\frac{1}{3} H_0 \frac{\partial^3 h}{\partial t^3} + \frac{\partial^3 v}{\partial t^2 \partial x} + \frac{\Delta x^2}{24} \frac{\partial^5 v}{\partial t^2 \partial x^3} \right) \\
 & + \frac{\Delta x^2}{8} \left(\frac{H_0}{3} \frac{\partial^3 v}{\partial x^3} + \frac{\partial^3 h}{\partial x^2 \partial t} + \frac{\Delta t^2}{24} \frac{\partial^5 h}{\partial x^2 \partial t^3} \right) + \dots
 \end{aligned} \tag{27}$$

A similar expansion for the truncation error may be obtained for Eq. (6b).

It is evident from an inspection of Eq. (27) that the truncation error approaches zero as the time step Δt and distance step Δx approach zero, i.e., convergence is attained as the time and distance steps are refined. This condition indicates that the four-point implicit difference equations are consistent with the linearized model equations.

The effect which the type of four-point implicit scheme has on the truncation error is seen readily if Eq. (27) is expressed in the following form:

$$E = O(\Delta t) + O(\Delta t^2) + O(\Delta x^2) \tag{28}$$

where O indicates "order of." When θ is unity, the truncation error is

$$E = O(\Delta t) + O(\Delta t^2) + O(\Delta x^2) \tag{29}$$

Thus, the backward implicit scheme is shown to have only first order accuracy due to the Δt term. When θ is 0.5, the truncation error is

$$E = O(\Delta t^2) + O(\Delta x^2) \tag{30}$$

The box implicit scheme is shown to have second order accuracy since both Δt and Δx are quadratic. It is significant that only when θ has a value of 0.5 is the truncation error of the higher, second order, degree of accuracy. An inspection of Eq. (28) indicates that as θ departs further from the value of 0.5 the truncation error becomes larger. This is due to the increasing contribution of the Δt term which has the leading coefficient $(2\theta-1)$.

3.3 Convergence Ratios

The conditions for convergence may be investigated quantitatively by determining the convergence ratio U/u . The model equations are again used

since an analytical solution to such a linear system of partial differential equations is possible.

The general solution of the linear system, Eqs. (6), may be determined by substituting the following complex Fourier components in Eqs. (6):

$$h = h^* e^{i(\sigma x + \beta t)} \quad (31a)$$

$$v = v^* e^{i(\sigma x + \beta t)} \quad (31b)$$

After differentiating, the following are obtained:

$$i\beta h^* + i\sigma H_0 v^* = 0 \quad (32a)$$

$$i\sigma g h^* + (i\beta + k)v^* = 0 \quad (32b)$$

Eliminating h^* from Eqs. (32) and dividing by v^* yields the following:

$$\beta^2 - ik\beta - gH_0\sigma^2 = 0 \quad (33)$$

Solving Eq. (33) for β , the following expression is obtained:

$$\beta = \sigma \left[\pm \sqrt{gH_0 - \left(\frac{k}{2\sigma}\right)^2} + i \frac{k}{2\sigma} \right] \quad (34)$$

Using Eq. (34), expressions for the physical wave damping and wave celerity (which shall be referred to as analytical damping and analytic celerity) may be obtained as follows:

$$\text{Analytical Damping} = e^{\text{Im}(\beta t)} = e^{-kt/2} \quad (35a)$$

$$\text{Analytical Celerity} = \frac{\text{Re}(\beta t)}{\sigma t} = \sqrt{gH_0 - \left(\frac{k}{2\sigma}\right)^2} \quad (35b)$$

The wave damping and celerity will now be determined for the four-point implicit difference equations. Referring to Eq. (17a) and recalling Eq. (12), the following expression is obtained:

$$e^{i\beta \Delta t} = r + is \quad (36)$$

where r and s are defined in Eqs. (17). After taking the logarithm of both sides of Eq. (36) and dividing by i , the following is obtained:

$$\beta\Delta t = \frac{1}{i} \ln(r+is) \quad (37)$$

however,

$$\ln(r+is) = \frac{1}{2} \ln(r^2+s^2) + i \tan^{-1} \left(\frac{s}{r} \right) \quad (38)$$

Therefore,

$$\beta\Delta t = \tan^{-1} \left(\frac{s}{r} \right) + \frac{1}{2i} \ln(r^2+s^2) \quad (39)$$

Using Eq. (39), expressions for the numerical wave damping and wave celerity may be obtained as follows:

$$\text{Numerical Damping} = e^{\text{Im}(\beta\Delta t)} = \frac{\sqrt{1+(2\theta-2)^2 a+(\theta-1)b}}{\sqrt{1+4\theta^2 a+\theta b}} \quad (40a)$$

$$\text{Numerical Celerity} = \frac{\text{Re}(\beta\Delta t)}{\sigma\Delta t} = \frac{1}{\sigma\Delta t} \tan^{-1} \left[\frac{\sqrt{16a-b^2}}{2+8\theta(\theta-1)a+2(\theta-1)b} \right] \quad (40b)$$

where a and b are given by Eqs. (16) and k is defined by Eq. (6c).

The convergence ratio is defined as the numerical solution divided by the analytical solution. Convergence ratios for wave damping and wave celerity are as follows:

$$C_d = \frac{\text{Numerical damping}}{\text{Analytical damping}} = \frac{\sqrt{1+(2\theta-2)^2 a+(\theta-1)b}}{\sqrt{1+4\theta^2 a+\theta b}} \cdot \frac{e^{-k\Delta t/2}}{e^{-k\Delta t/2}} \quad (41a)$$

$$C_c = \frac{\text{Numerical celerity}}{\text{Analytical celerity}} = \frac{\tan^{-1} \left[\frac{\sqrt{16a-b^2}}{2+8\theta(\theta-1)a+2(\theta-1)b} \right]}{\sigma\Delta t \sqrt{gH_o - \left(\frac{k}{2\sigma} \right)^2}} \quad (41b)$$

In order to facilitate the analysis of Eqs. (41), it is advantageous to nondimensionalize them. This can be accomplished by defining the following dimensionless parameters:

$$D_L = \frac{L}{\Delta x} \quad (42a)$$

$$D_c = \frac{\Delta t}{\Delta x} \sqrt{gH_0} \quad (42b)$$

$$D_f = k\Delta t = \frac{k}{\sigma \sqrt{gH_0}} \quad (42c)$$

where D_c is the dimensionless measure of the spatial discretization of the wave, D_L is the dimensionless Courant parameter, and D_f is a dimensionless friction parameter. Using these parameters, the following relations may be obtained:

$$a = gH_0 \left(\frac{\Delta t}{\Delta x}\right)^2 \tan^2(\sigma \Delta x/2) = (D_c \tan \pi/D_L)^2 \quad (43a)$$

$$b = k \Delta t = D_f \quad (43b)$$

$$\frac{k}{\sigma} = D_f \sqrt{gH_0} \quad (43c)$$

$$\sigma \Delta t \sqrt{gH_0 - \left(\frac{k}{2\sigma}\right)^2} = \frac{2\pi}{D_L} D_c \sqrt{1 - (D_f/2)^2} \quad (43d)$$

Substitution of Eqs. (43) in Eqs. (41) yields the following dimensionless expressions of the convergence ratios for wave damping and wave celerity:

$$C_d = \frac{\sqrt{\frac{1 + (2\theta - 2)^2 (D_c \tan \pi/D_L)^2 + (\theta - 1) D_f}{1 + 4\theta^2 (D_c \tan \pi/D_L)^2 + \theta D_f}}}{e^{-D_f/2}} \quad (44a)$$

$$C_c = \frac{\tan^{-1} \left[\frac{\sqrt{16 (D_c \tan \pi/D_L)^2 - D_f^2}}{2 + 8\theta(\theta - 1) (D_c \tan \pi/D_L)^2 + (2\theta - 1) D_f} \right]}{\frac{2\pi}{D_L} D_c \sqrt{1 - (D_f/2)^2}} \quad (44b)$$

From Eqs. (44), it can be seen that C_d and C_c are functions of θ , D_L , D_f , and D_f^C . Accordingly, C_d and C_c were computed for the following range of parameter values: $\theta=0.5$ and 1.0 , $3 \leq D_L \leq 1000$, $1 \leq D_f \leq 100$, and $0 \leq D_f^C \leq 1.0$. The plotted results are presented in Figs. 2, 3, 4, and 5.

In Fig. 2, the convergence ratios C_d and C_c are plotted against D_L for increasing values of the Courant parameter D_f^C . These curves are associated with a θ value of 0.5 and a D_f value of zero, i.e., the convergence ratio curves apply to the box four-point scheme for a condition of negligible friction. In the upper graph, the convergence ratio C_d is unity for all values of D_f and D_L . This indicates that the numerical wave and the analytical wave damping have identically the same value, which in the case of no friction, is zero. In the lower graph, the celerity convergence ratio C_c varies depending on the values of D_f and D_L . In general, for a given D_L , C_c becomes less than unity as D_f increases; however, the curves tend to converge to unity as D_L increases. Thus, the numerical wave tends to lag the analytical wave as D_f increases, i.e., as the time step increases. This trend is independent of the value of Δx for a given wave length; but as the wave length decreases, the error in the numerically computed wave celerity increases in magnitude.

In Fig. 3, C_d and C_c are plotted against D_L for increasing values of D_f^C . These curves are associated with a θ of 0.5 and a D_f of 0.4. Unlike Fig. 2, C_d departs from unity. It can be seen that the numerical wave damping can be greater than that of the analytical solution and that this trend is related directly to D_f and indirectly to D_L . The lower graph of Fig. 3 is quite similar to that in Fig. 2, indicating that the celerity convergence ratio is not sensitive to the friction parameter D_f .

Fig. 4 shows the graphs for C_d and C_c for the box scheme when D_f has a value of 1.0. The curves are similar to those in Fig. 3 except for the amplification of the C_d curves. This indicates that C_d tends to depart further from unity as D_f increases, i.e., the numerical wave damping becomes greater than the analytical damping as frictional effects become more important. A comparison of the C_c curves in Figs. 2, 3, and 4 indicates that the celerity convergence ratio is affected very little by friction.

In Fig. 5, the convergence ratios are presented for the backward implicit four-point scheme where θ is unity and D_f is zero. A comparison of these graphs with those in Fig. 2 illustrates the effect of the θ value on the convergence ratios. From Fig. 5, it is seen that in the fully implicit scheme the damping convergence ratio becomes less than unity as D_f^C increases and D_L decreases, whereas in Fig. 2, the box scheme has a damping convergence ratio of unity. Although not shown herein, the effect of friction on the C_d curves for the backward implicit scheme is similar to that for the box scheme, i.e., the error in the extent of damping increases as D_f increases. As for the celerity convergence ratio, a comparison of Figs. 2 and 5 indicates the C_c departs somewhat further from unity for the backward implicit scheme than for the box scheme.

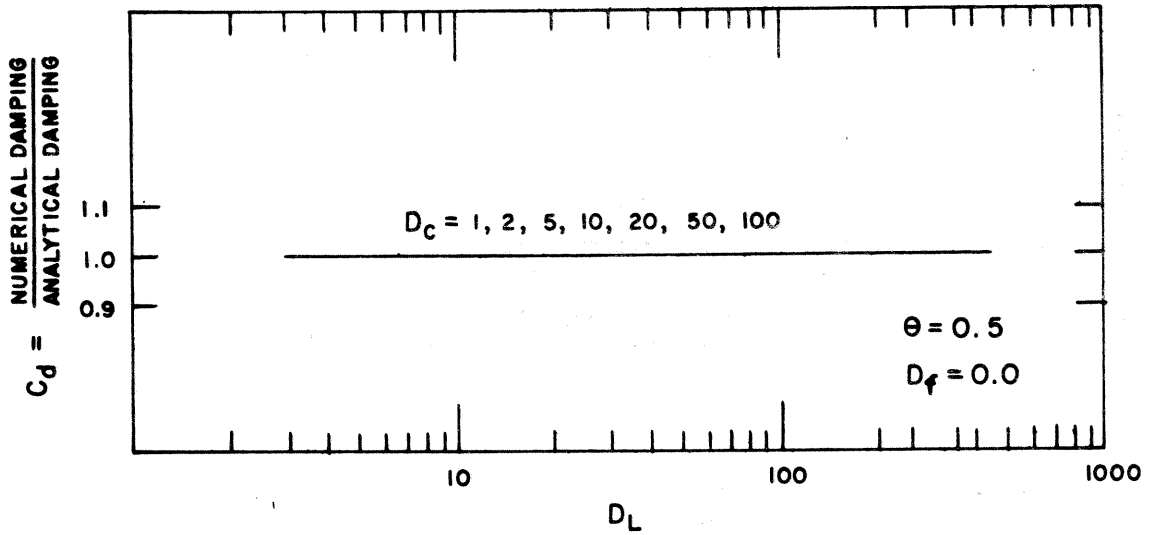


Fig. 2a - Damping Convergence Ratio, C_d , Against D_L for Box Scheme with Variations in D_c and $D_f = 0.0$.

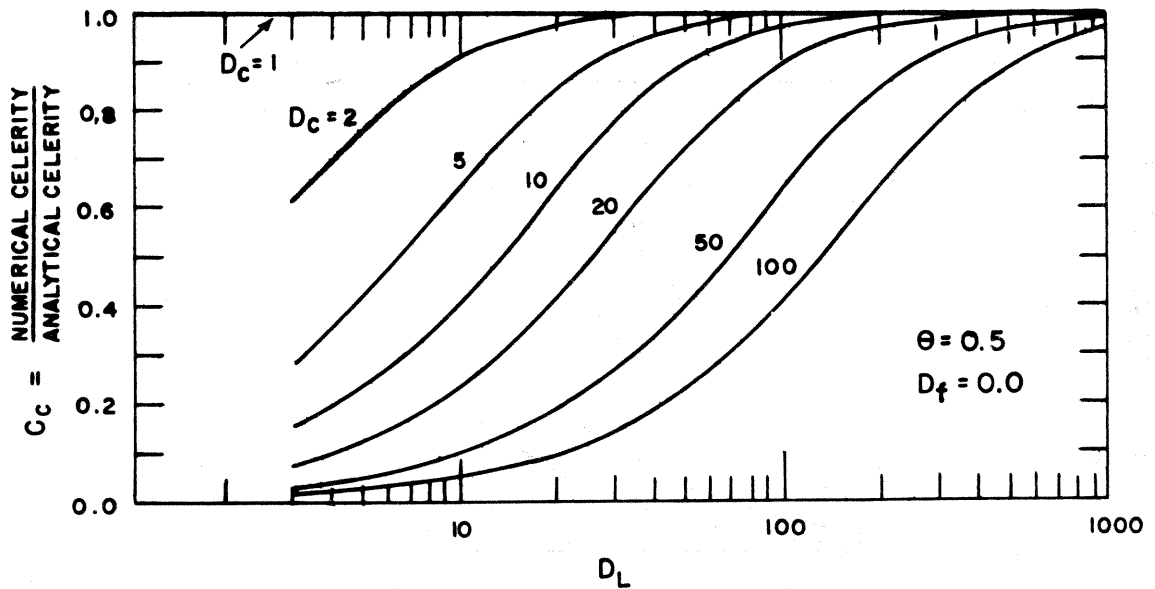


Fig. 2b - Celerity Convergence Ratio, C_c , Against D_L for Box Scheme with Variations in D_c and $D_f = 0.0$

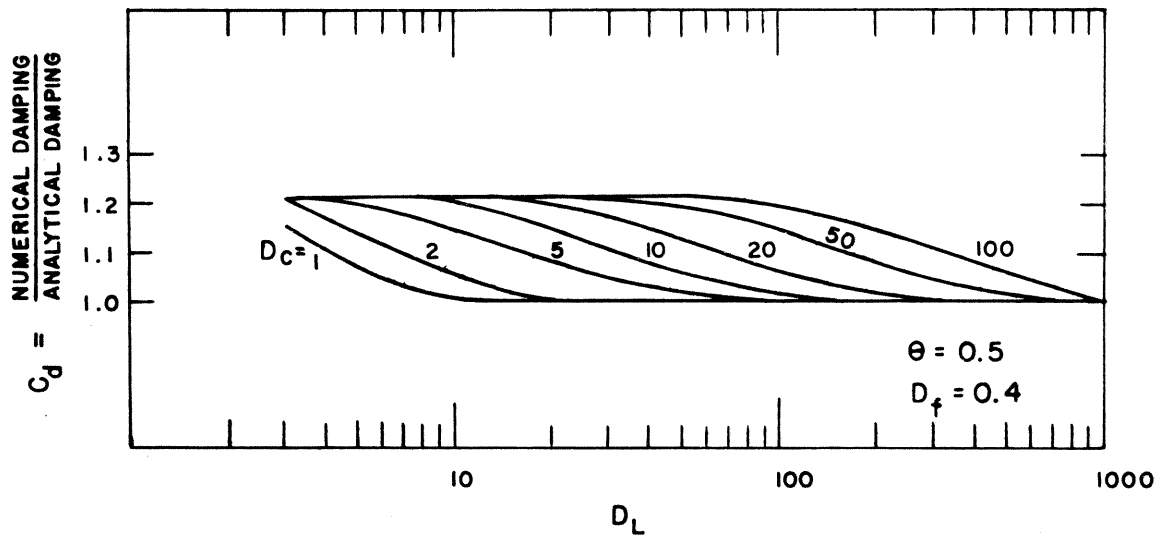


Fig. 3a - Damping Convergence Ratio, C_d , Against D_L for Box Scheme with Variations in D_c and $D_f = 0.4$.

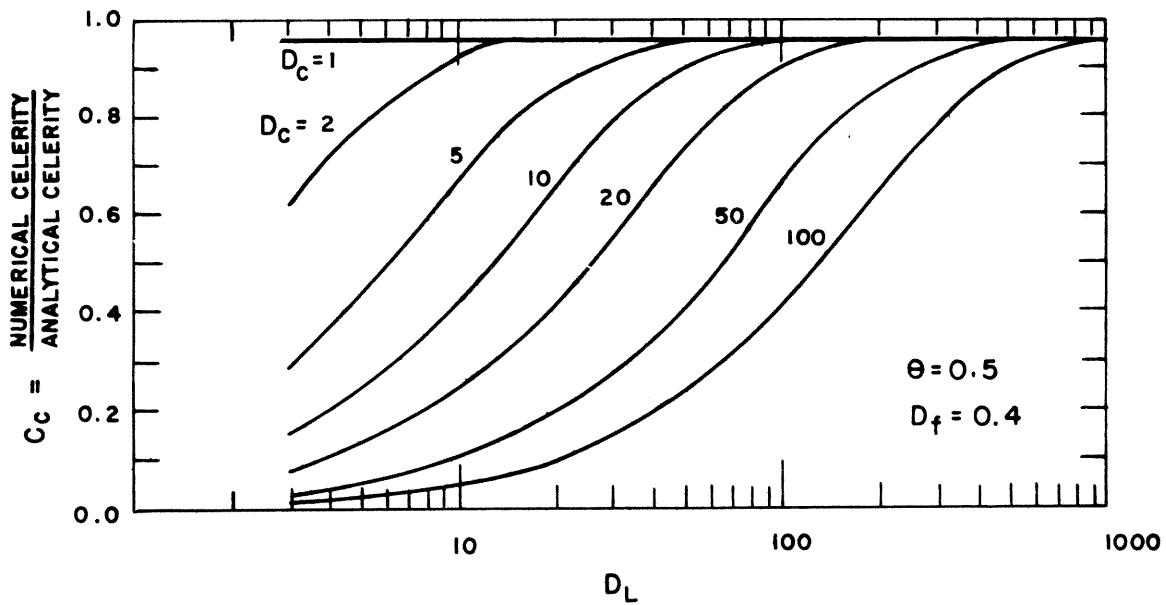


Fig. 3b - Celerity Convergence Ratio, C_c , Against D_L for Box Scheme with Variations in D_c and $D_f = 0.4$

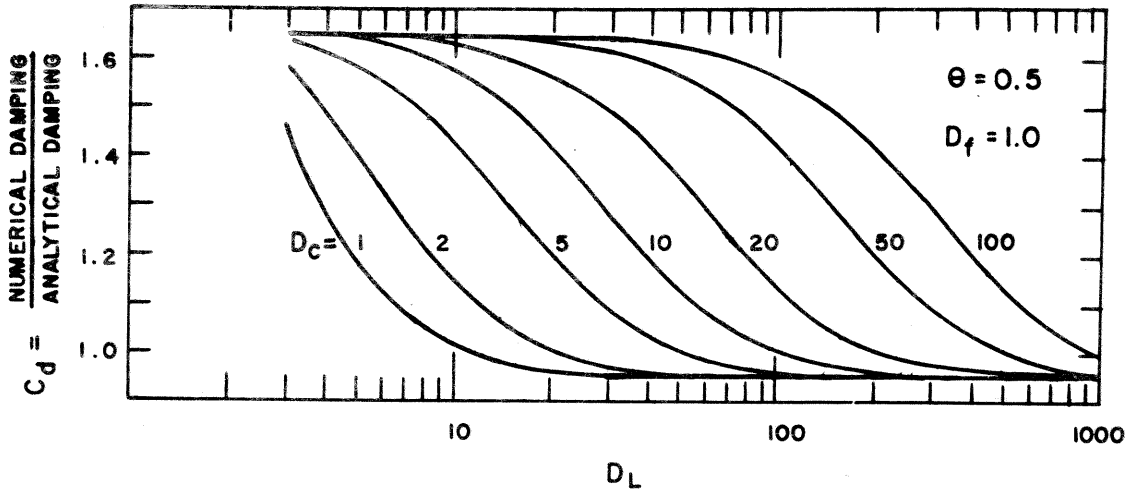


Fig. 4a - Damping Convergence Ratio, C_d , Against D_L for Box Scheme with Variations in D_c and $D_f = 1.0$.

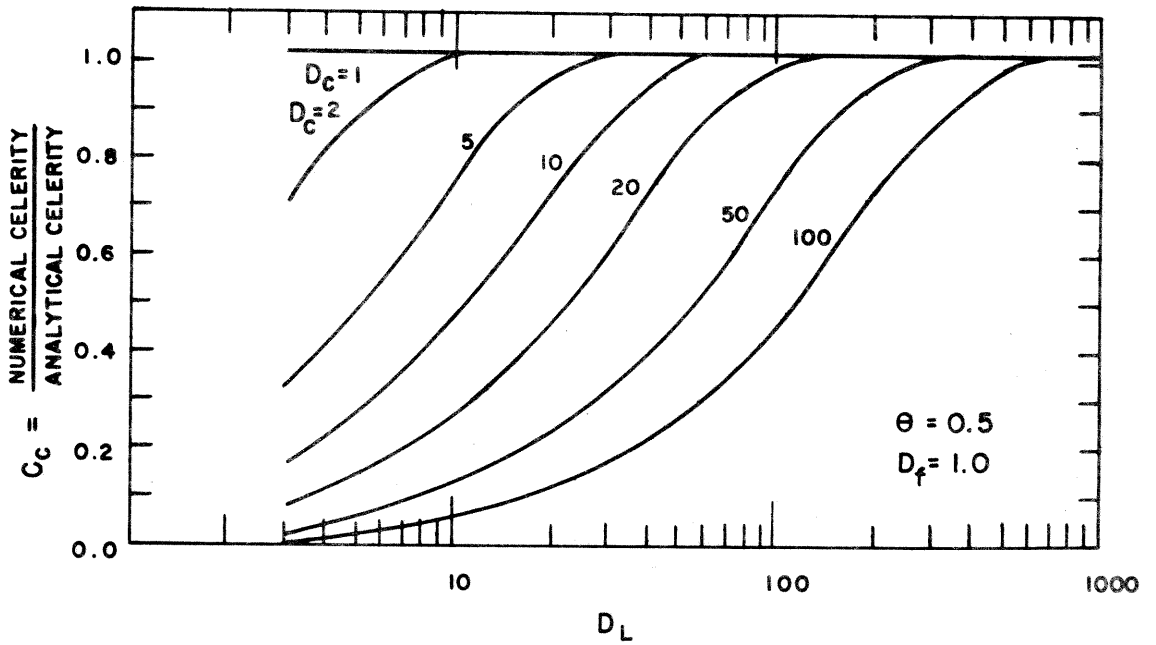


Fig. 4b - Celerity Convergence Ratio, C_c , Against D_L for Box Scheme with Variations in D_c and $D_f = 1.0$.

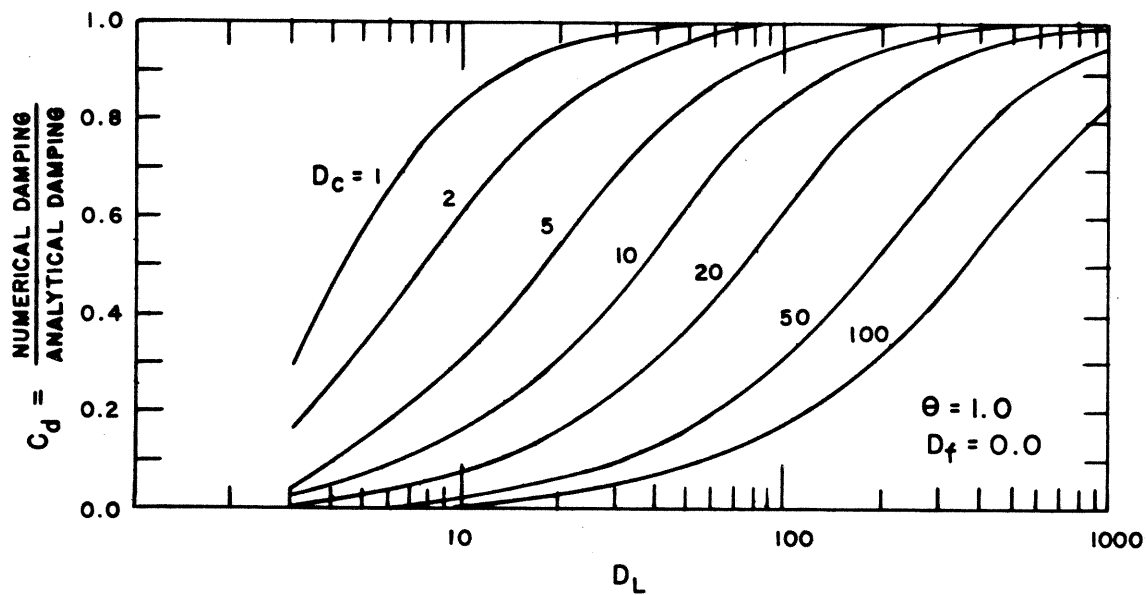


Fig. 5a - Damping Convergence Ratio, C_d , Against D_L for Backward Implicit Scheme with Variations in D_c and $D_f = 0.0$

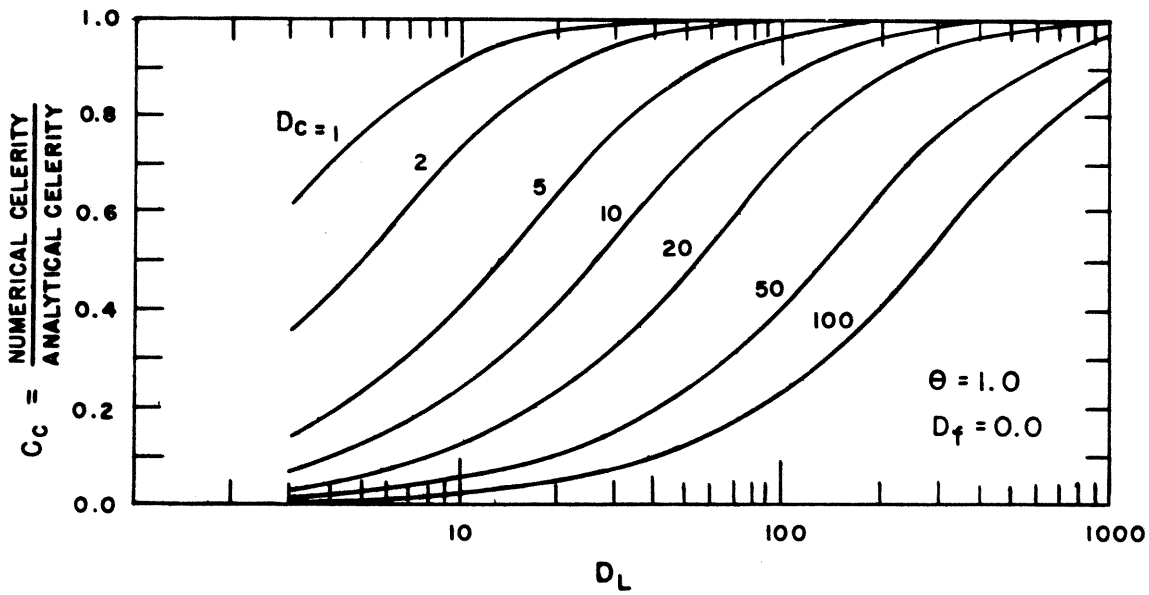


Fig. 5b - Celerity Convergence Ratio, C_d , Against D_L for Backward Implicit Scheme with Variations in D_c and $D_f = 0.0$

3.4 Mass Conservation

A good indicator of the convergence of finite difference schemes for the unsteady flow equations is the extent to which the scheme conserves mass between the spatial boundaries of the system. If the finite difference approximations given in Eqs. (4) are substituted in Eq. (1a), wherein q is assumed to be zero, the following difference equation for the conservation of mass is obtained:

$$\frac{A_m^{n+1} + A_{m+1}^{n+1} - A_m^n - A_{m+1}^n}{2\Delta t} + \theta \left[\frac{(AV)_{m+1}^{n+1} - (AV)_m^{n+1}}{\Delta x} \right] + (1-\theta) \left[\frac{(AV)_{m+1}^n - (AV)_m^n}{\Delta x} \right] = 0 \quad (45)$$

If all the terms along the x -axis from $m=1$ to $m=M-1$ (i.e., from the upstream to the downstream boundaries of the system) are summed, the following equation is obtained:

$$\frac{\Delta x}{\Delta t} \sum_{m=1}^{m=M-1} \left[\frac{(A_m^{n+1} + A_{m+1}^{n+1})}{2} - \frac{(A_m^n + A_{m+1}^n)}{2} \right] = \theta [(AV)_1^{n+1} - (AV)_M^{n+1}] + (1-\theta) [(AV)_1^n - (AV)_M^n] \quad (46)$$

If $\theta=0.5$, Eq. (46) becomes:

$$\frac{\Delta x}{\Delta t} \sum_{m=1}^{m=M-1} \left[\frac{(A_m^{n+1} + A_{m+1}^{n+1})}{2} - \frac{(A_m^n + A_{m+1}^n)}{2} \right] = \left[\frac{(AV)_1^n + (AV)_1^{n+1}}{2} \right] - \left[\frac{(AV)_M^n + (AV)_M^{n+1}}{2} \right] \quad (47)$$

which can be written in the following form:

$$\frac{\text{Change in Volume}}{\Delta t} = \text{Inflow} - \text{Outflow} \quad (48)$$

Thus, over one time step, the four-point box implicit scheme conserves the mass within the spatial boundaries if the mass which enters or leaves the system through the boundaries is taken into account.

If $\theta=1$, Eq. (46) becomes:

$$\frac{\Delta x}{\Delta t} \sum_{m=1}^{m=M-1} \left[\frac{(A_m^{n+1} + A_{m+1}^{n+1})}{2} - \frac{(A_m^n + A_{m+1}^n)}{2} \right] = (AV)_1^{n+1} - (AV)_M^{n+1} \quad (49)$$

In Eq. (49), the right-hand term does not represent an average value during the time step as it does in Eq. (47). Hence, the backward implicit scheme is not as good a representation of the conservation of mass during an interval of time as is the box scheme. This may be extended to apply to all θ values which depart from a value of 0.5, and the extent to which the scheme does not conserve mass is proportional to the departure of θ from a value of 0.5.

3.5 Momentum Conservation

Substitution of Eqs. (4), with $\theta=0.5$, in Eq. (1b), with $q=0$, gives the following difference equation for the conservation of momentum:

$$\frac{v_m^{n+1} + v_{m+1}^{n+1} - v_m^n - v_{m+1}^n}{2\Delta t} + \frac{1}{2} \left(\frac{v_{m+1}^{2n+1} - v_m^{2n+1} + v_{m+1}^{2n} - v_m^{2n}}{2\Delta x} \right) + g \left[\frac{(h_{m+1}^{n+1} - h_m^{n+1} + h_{m+1}^n - h_m^n)}{2\Delta x} - s_o + \frac{(s_{f_m}^{n+1} + s_{f_{m+1}}^{n+1} + s_{f_m}^n + s_{f_{m+1}}^n)}{4} \right] = 0 \quad (50)$$

Summing all the terms along the x-axis from $m=1$ to $m=M-1$ gives:

$$\frac{1}{2\Delta t} \sum_{m=1}^{m=M-1} (v_m^{n+1} + v_{m+1}^{n+1} - v_m^n - v_{m+1}^n) + \frac{1}{2} \left[\frac{(v_M^{2n+1} - v_1^{2n+1})}{2\Delta x} + \frac{(v_M^{2n} - v_1^{2n})}{2\Delta x} \right] + g \left[\frac{(h_M^{n+1} - h_1^{n+1})}{2\Delta x} + \frac{(h_M^n - h_1^n)}{2\Delta x} - s_o \right] + \frac{g}{4} \sum_{m=1}^{m=M-1} (s_{f_m}^{n+1} + s_{f_{m+1}}^{n+1} + s_{f_m}^n + s_{f_{m+1}}^n) = 0 \quad (51)$$

Thus, over one time step, the box scheme conserves the momentum within the spatial boundaries if the momentum which enters or leaves the system through the boundaries is taken into account. This is demonstrated by Eq. (51) in that the finite difference expressions for the spatial derivatives ($\partial v^2/\partial x$ and $\partial h/\partial x$) do not contain contributions from within the boundaries of the system. If the term $(1/2 \partial v^2/\partial x)$ were replaced with its equivalent $(v \partial v/\partial x)$, the preceding analysis would show that contributions from within the boundaries are contained within the finite difference expression of this spatial derivative term. Thus, Eq. (1b) is a preferred form of the momentum equation for four-point finite difference solutions.

3.6 Numerical Experiments

The rate of convergence of difference schemes may be investigated via numerical experiments in which the solutions for various size time steps and wave conditions are compared. The results of such a study of the implicit four-point schemes for the unsteady flow equations was reported by Fread [1973a]. A summary of those numerical experiments follows:

If the finite difference operators defined by Eqs. (4) are substituted in Eqs. (1) wherein q is assumed negligible, the following implicit four-point difference equations are obtained:

$$\frac{A_m^{n+1} + A_{m+1}^{n+1} - A_m^n - A_{m+1}^n}{2\Delta t} + \theta \left[\frac{(AV)_{m+1}^{n+1} - (AV)_m^{n+1}}{\Delta x} \right] + (1-\theta) \left[\frac{(AV)_{m+1}^n - (AV)_m^n}{\Delta x} \right] = 0 \quad (52a)$$

$$\frac{V_m^{n+1} + V_{m+1}^{n+1} - V_m^n - V_{m+1}^n}{2\Delta t} + \theta \left\{ \frac{(V^2)_{m+1}^{n+1} - (V^2)_m^{n+1}}{2\Delta x} + g \left[\frac{(H)_{m+1}^{n+1} - (H)_m^{n+1}}{\Delta x} - S_o + \frac{(S_f^m + S_f^{m+1})^{n+1}}{2} \right] \right\} \\ + (1-\theta) \left\{ \frac{(V^2)_{m+1}^n - (V^2)_m^n}{2\Delta x} + g \left[\frac{(H)_{m+1}^n - (H)_m^n}{\Delta x} - S_o + \frac{(S_f^m + S_f^{m+1})^n}{2} \right] \right\} = 0 \quad (52b)$$

where

$$S_f = \frac{n^2 |V| V}{2.21 R^{4/3}} \quad (52c)$$

Eqs. (52) form a system of two algebraic equations which are nonlinear with respect to the unknowns, the values of H and V at the net points $(m, n+1)$ and $(m+1, n+1)$. The terms A and S_f are known functions of H and/or V . The terms associated with the net points (m, n) and $(m+1, n)$ are known from either the initial conditions or previous computations. The two equations cannot be solved for the unknowns since there are two more unknowns than equations; however, by considering all M number of points along the x -axis simultaneously, a solution may be obtained. In this way, a total of $(2M-2)$ equations with $2M$ unknowns may be formulated by applying Eqs. (52) recursively to the $(M-1)$ rectangular grids along the x -axis. The boundary conditions at the upstream

and downstream extremities of the channel reach provide two additional equations which are necessary for the system of equations to be sufficiently proposed to yield a solution. The resulting system of 2M nonlinear equations with 2M unknowns must be solved by an iterative procedure. A functional iterative process, called Newton-Raphson Iteration [Isaacson and Keller, 1966; Amein and Fang, 1970], is used to solve the nonlinear system. The iterative process may be improved by using parabolic extrapolation to obtain the first approximation of the solution from solutions determined at previous times. The coefficient matrix of the linearized system of equations has a banded structure which lends itself to very efficient solution algorithms, e.g., [Fread, 1970].

Truncation errors, related to the magnitude of the Δt time step, arise during the integration of the implicit difference equations. The truncation errors distort the computed transient via numerical dispersion and damping, which in combination will be called "numerical distortion." Also, as will be shown later, the characteristics of the discharge hydrograph at the upstream extremity of the channel reach significantly affect the accuracy of the solution.

The characteristics of the numerical distortion can be investigated via numerical experiments in which Eqs. (52) are applied to upstream boundary transients described by the following four-parameter, Pearson Type III distribution:

$$Q(t) = Q_0 \left[1 + (\rho - 1) \left(\frac{t}{\tau} \right)^{\frac{1}{\gamma - 1}} e^{-(1-t/\tau)^{\frac{1}{\gamma - 1}}} \right] \quad (53a)$$

in which

$$\rho = Q_{\max} / Q_0 \quad (53b)$$

$$\gamma = \tau_g / \tau \quad (53c)$$

The terms in the above equations are defined as follows: $Q(t)$ = discharge at any time (t); Q_0 = initial steady discharge as computed by the Manning equation; Q_{\max} = maximum discharge at the upstream boundary during the transient flow condition; τ = time of occurrence of Q_{\max} ; τ_g = time associated with the center of gravity of the upstream hydrograph; $\rho = Q_{\max} / Q_0$ = hydrograph amplification coefficient; and γ = a skewness coefficient of the upstream hydrograph.

The downstream boundary condition is specified by the following implicit stage-velocity relationship which is corrected for transient effects:

$$V = \frac{1.486}{n} \left(\frac{A}{P}\right)^{2/3} S_f^{1/2} \quad (54a)$$

in which P = the wetted perimeter of the channel cross section and,

$$S_f = S_o - \frac{\partial H}{\partial x} - \frac{1}{g} \frac{\partial V}{\partial t} - \frac{1}{2g} \frac{\partial V^2}{\partial x} \quad (54b)$$

This boundary condition allows the transient to pass the downstream extremity of the channel reach without the occurrence of numerical reflection.

The primary objective of the numerical experiments presented herein is to study the effect of relatively large time steps on the solution of the implicit difference equations for transients having durations of the order of days and even weeks. Accordingly, selected parameters describing the physical characteristics of the channel reach are held constant except in special instances where a single parameter is perturbed in order to determine its effect on the results. The selected channel parameters are as follows: channel reach length (L) = 100 miles; channel bottom slope (S_o) = 1/5280 ft per ft; Manning roughness coefficient (n) = 0.03; wide rectangular cross-section, hence the surface width (B) may be taken as unity; L/Δx=10; and initial depth of flow (Y_o) = 5 ft. Convergence criteria for H and V in the

iterative solution were chosen as: $|H^{k'+1} - H^{k'}| \leq 1 \times 10^{-6}$ and $|V^{k'+1} - V^{k'}| \leq 1 \times 10^{-6}$, where the superscript k' denotes the number of iterations.

The effect of the magnitude of the time step on the accuracy of the computed solutions is determined by systematically increasing the time step from Δt_c, a relatively small value in the order of minutes, to a relatively large value of 12 hrs. The Δt_c time step is the maximum size time step that can be used in the explicit finite difference method; it is computed from the Courant stability condition, Eq. (2). The stage hydrographs obtained using Δt_c in Eqs. (52) are considered the standards to which the solutions computed with Δt time steps of 1, 3, 6, and 12 hrs are compared.

Deviations from the standard hydrographs are measured by the following relative root mean square error (S_e) and relative error of the peak (P_e) of the hydrographs:

$$S_e = \frac{100 \left[\sum_{j=1}^{j=n} (y_j - y_{s_j})^2 \right]^{1/2}}{n^{1/2} y_{s_p}} \quad (55)$$

$$P_e = 100(1 - y_p / y_{s_p}) \quad (56)$$

in which n' = total number of hydrograph values being compared, y_j = stage value computed with a particular Δt time step, y_{s_j} = stage value computed with a Δt_c time step, y_p = maximum (peak) value of Y_j , and y_{s_p} = maximum value of \bar{y}_{s_j} .

Figs. 6 and 7 illustrate typical numerical distortions of the computed hydrographs at the downstream boundary for two variations in the upstream boundary condition. In Fig. 6, the time of rise (τ) is 48 hrs, while in Fig. 7, τ is 120 hrs. The hydrographs obtained with a time step of 12 hrs differ from those computed with a time step of 0.5 hr. The rising limb of the former occurs earlier than the latter, while the falling limb is delayed and the peak is attenuated. The distortion is more pronounced in Fig. 6 than in Fig. 7 for the same values of Δt and θ . Also, for a single τ value, the distortion is significantly greater for $\theta=1.0$ than for $\theta=0.55$.

A quantitative evaluation of the numerical distortion, in terms of S_e and P_e , is shown in Fig. 8. The influence of θ and τ on the degree of distortion is significant. This was also observed for other test hydrographs. Thus, it may be concluded that the lower range of allowable θ values minimizes the distortion (dispersion and attenuation) which results from the use of large time steps in the integration of the implicit difference equations. Also, the degree of distortion becomes less as the time of rise of the input hydrograph increases. Several correlations of S_e with the size of the Δt time step are shown in Fig. 9. The correlations are given for various τ and ρ values of the upstream boundary hydrograph. The S_e error is associated with the stage hydrographs computed at the downstream boundary of the 100-mile channel reach described previously.

An examination of Fig. 9 yields the following information concerning the numerical distortion resulting from the use of Δt time steps considerably larger than those determined from the Courant condition, Eq. (2).

- 1) The magnitude of S_e increases with the size of the Δt time step;
- 2) as τ , the time of rise of the upstream hydrograph increases, the slopes of the $(S_e, \Delta t)$ curves decrease;
- 3) the magnitude of S_e is less than 1% for $\tau \geq 96$ hrs and $\Delta t \leq 12$ hrs.

The solid curves in Fig. 9 are applicable for a θ of 0.55, a value chosen so as to minimize the numerical distortion while conservatively insuring the absence of a computational mode (weak stability) in the computations. The dashed portions of the curves are applicable to θ values greater than 0.55 which are required for numerical stability since lesser values of θ cause instabilities to arise in the iterative solution of the nonlinear difference equations. The selected θ values are optimal in that the magnitude of numerical distortion is minimized while numerical stability is achieved. The optimal θ values vary with Δt and τ . From an inspection of Fig. 9, it

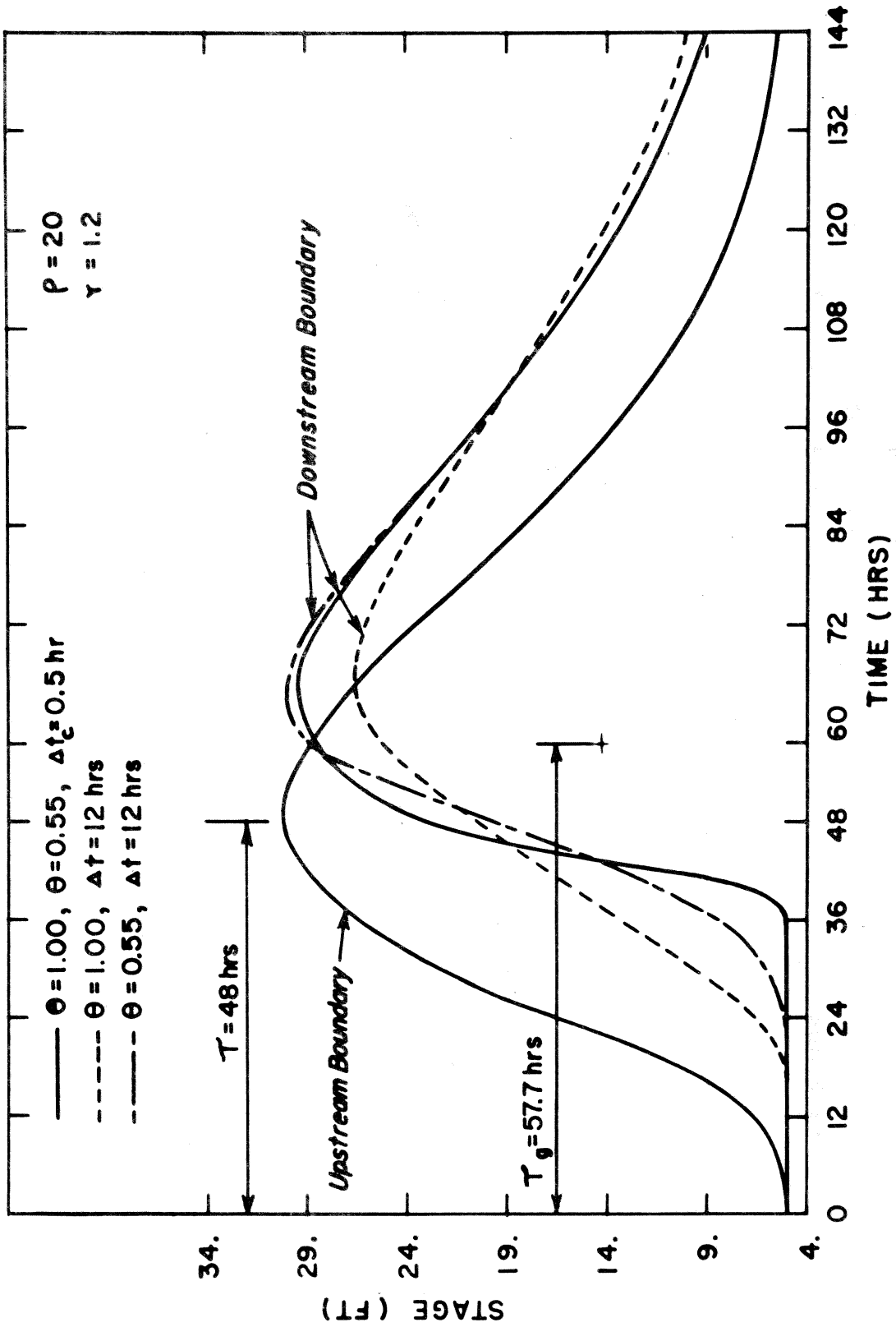


Fig. 6. Distortion of Computed Downstream Stage Hydrograph for Large Δt Steps When θ is varied and $t=48$ Hours

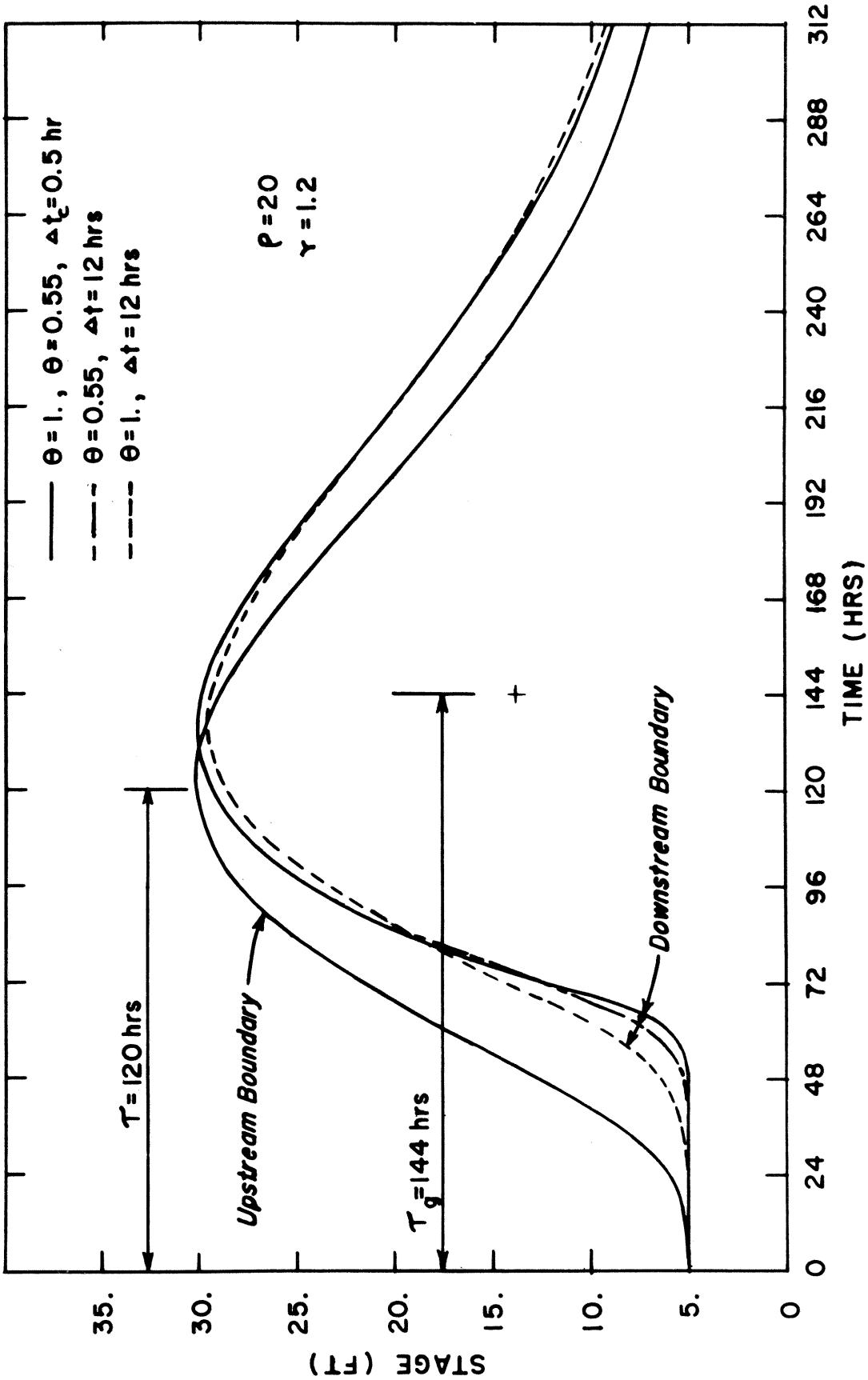


Fig. 7. Distortion of Computed Downstream Stage Hydrograph for Large Δt Steps When θ is Varied and $\tau = 120$ Hours

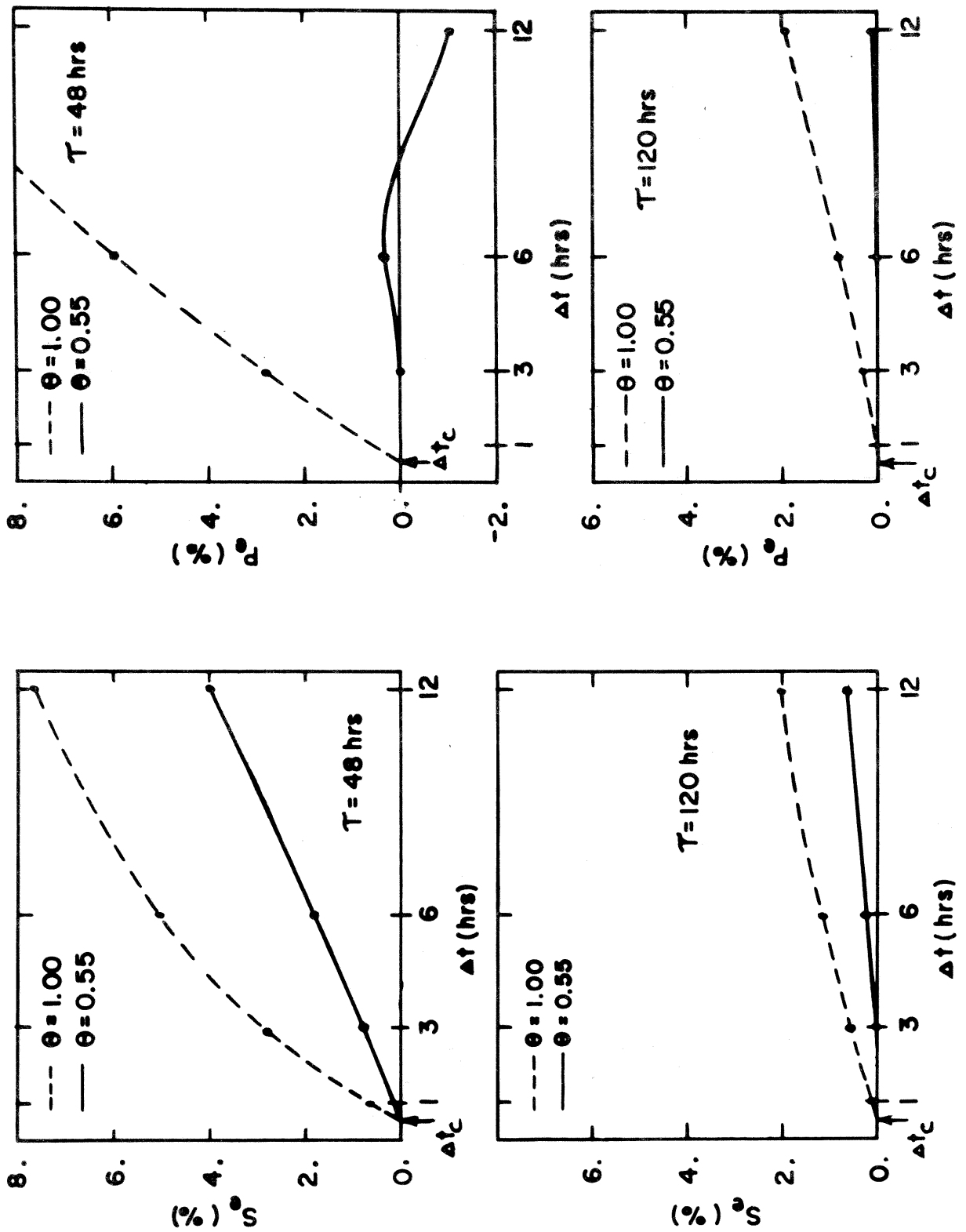
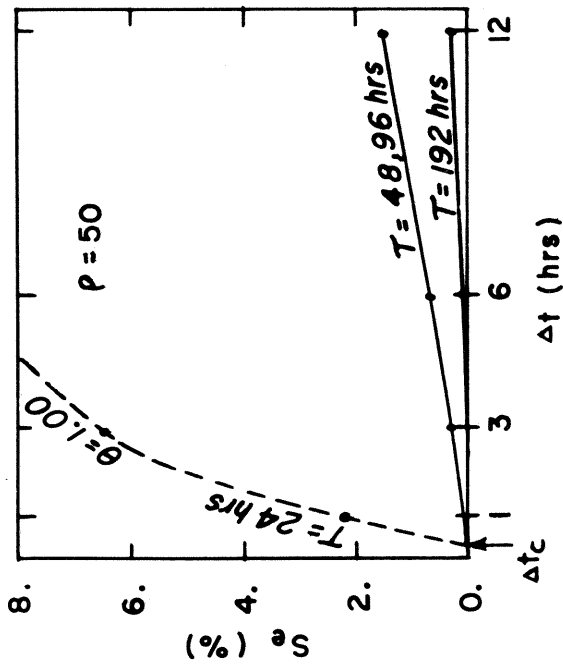
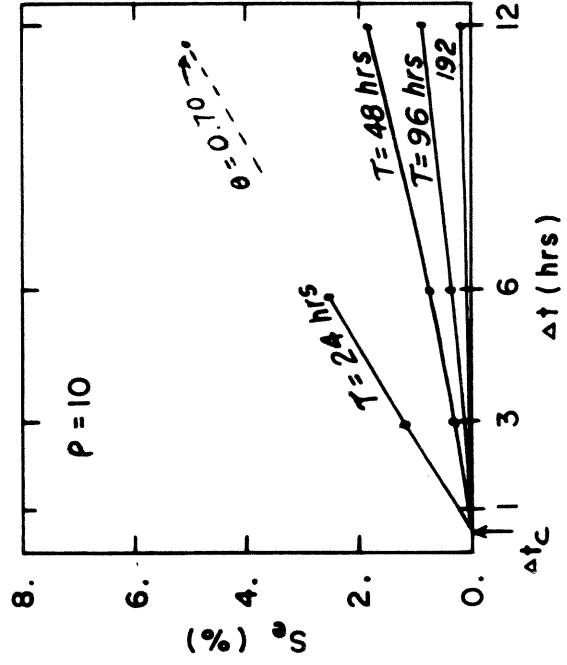
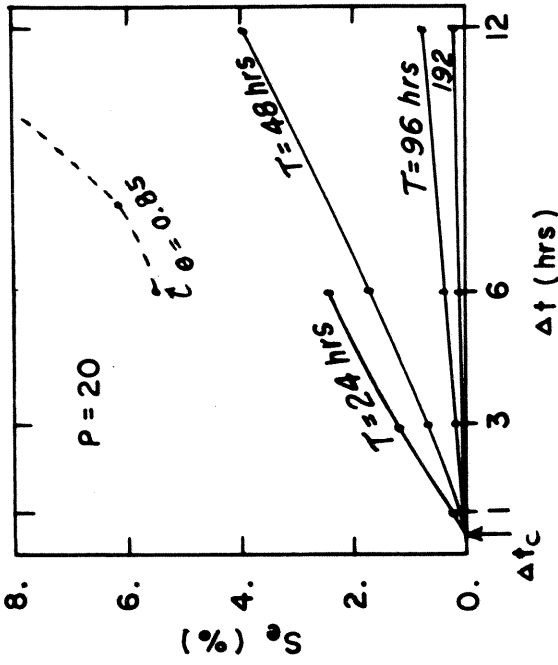


Fig. 8. Effect of θ and τ on the Distortion of the Computed Stage Hydrograph at the Downstream Boundary for Various Δt Time Steps Having $\rho=20$ and $\gamma=1.2$



— $\theta = 0.55$

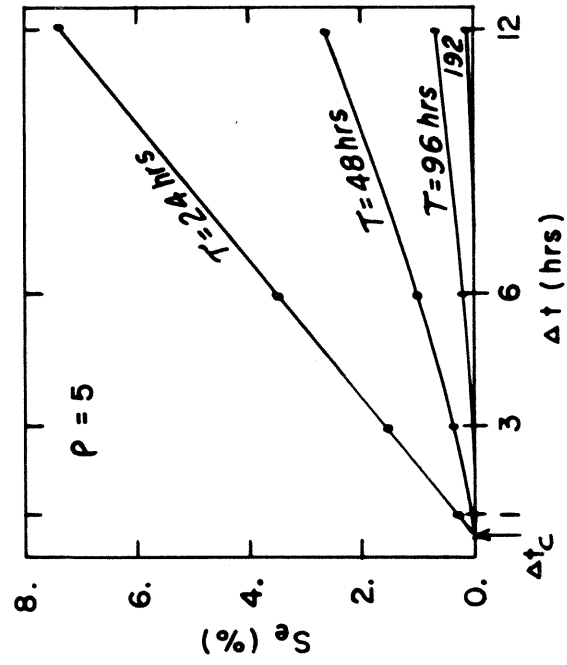


Fig. 9. Correlation of S_e Error (for the Stage at the Downstream Boundary) with the Δt Time Step for Various Upstream Boundary Hydrographs Having $\gamma=1.2$

can be seen that the tendency for stable numerical computations decreases with increasing values of Δt and with decreasing values of θ and τ .

The effect of the Δt time step size on the attenuation of the computed stage hydrographs at the downstream boundary is presented in Fig. 10 for various combinations for τ and ρ . In Fig. 10, P_e is negligible for τ values greater than 48 hrs; however, P_e can be significant for $\Delta t \gg 3$ hr when $\tau \leq 48$ hrs.

The results presented thus far are applicable for the constant channel parameters selected previously. In order to determine if the numerical distortion resulting from large time steps is sensitive to the values of the channel parameters, these are perturbed and the resulting effects on S_e and P_e are observed. The observed effects may be summarized by the following approximation:

$$(S_e', P_e') = \eta \cdot (S_e, P_e) \quad (57)$$

in which the prime superscript denotes the magnitude of S_e or P_e associated with any channel parameter (ψ') having a different value than the constant value of the corresponding parameter (ψ) for which Figs. 9 and 10 are applicable. The correction factor η is presented in Fig. 11 for the various channel parameters in terms of the ratio, ψ'/ψ . It can be observed from Fig. 11 that the numerical distortion increases when either the channel length, L , or the Manning roughness factor, \bar{n} , increase; and decreases when either the magnitude of the initial depth of flow, Y_o , or the channel bottom slope, S_o , increase. The magnitude of the numerical distortion increases with the distance from the upstream boundary to the channel location in question.

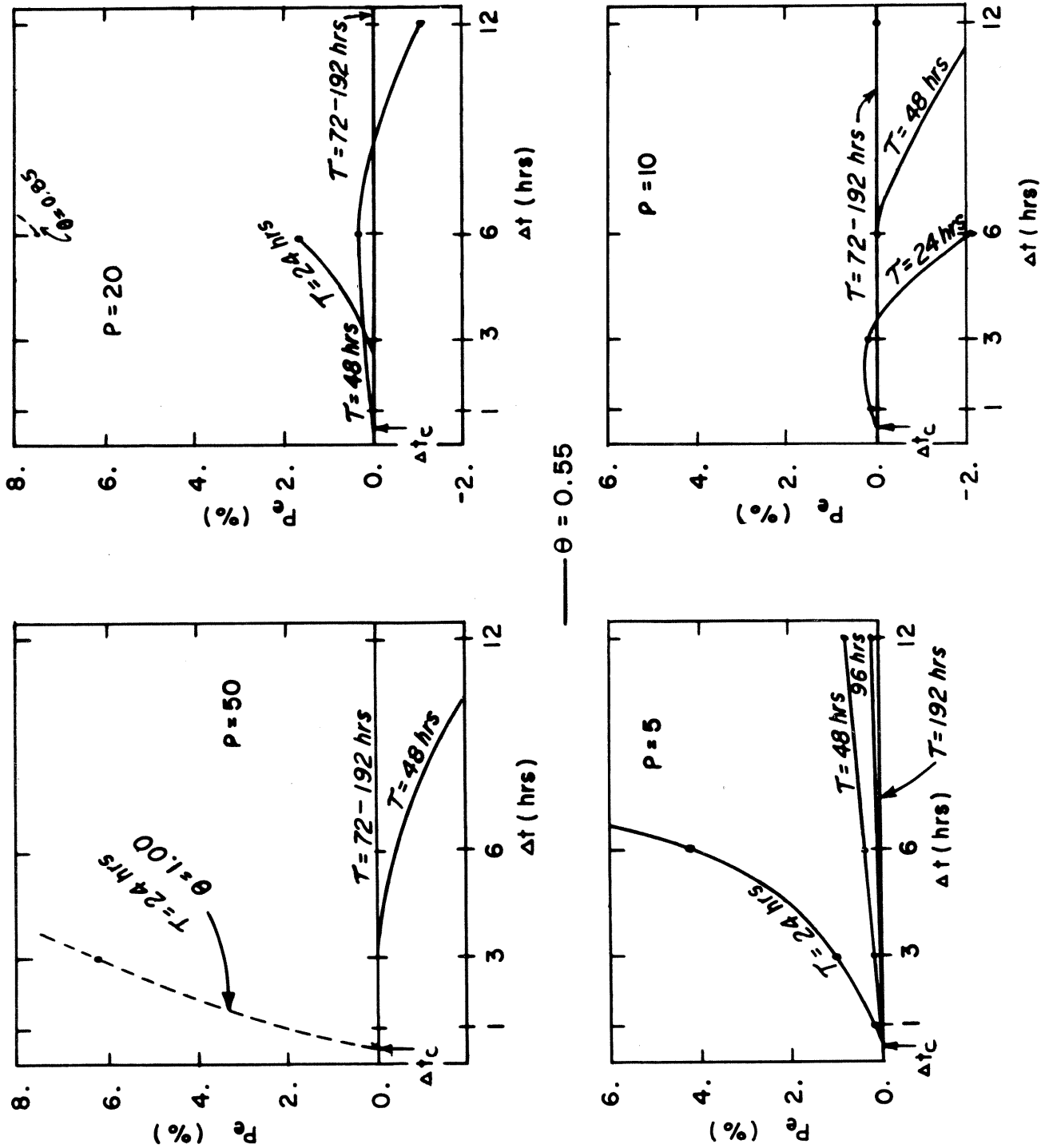


Fig. 10. Correlation of P_e Error (for the Stage at the Downstream Boundary) with the Δt Time Step^e for Various Upstream Boundary Hydrographs Having $\gamma = 1.2$

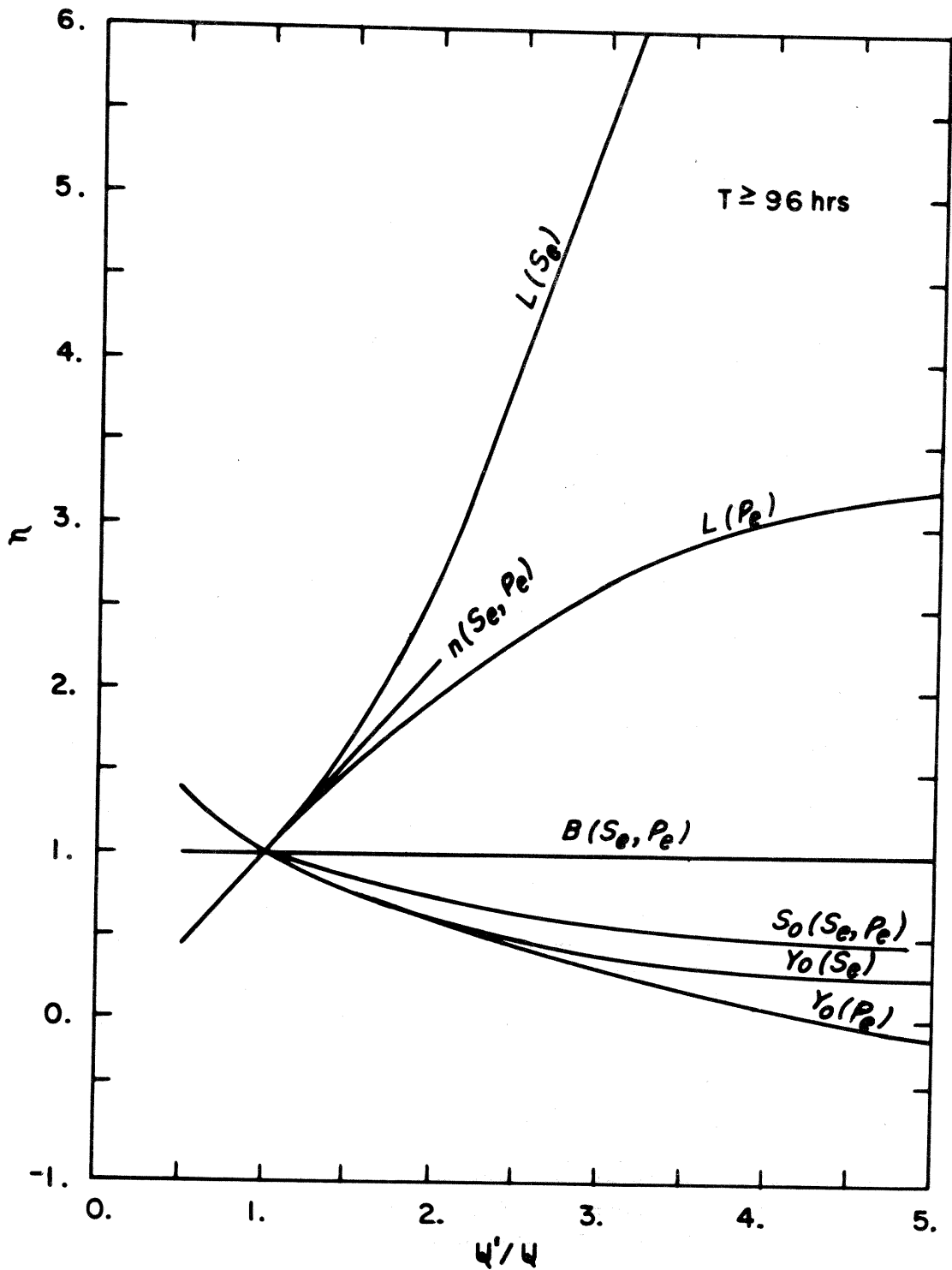


Fig. 11. Correction Factor, η , for Determining the Effect of Various Channel Parameters on the Numerical Distortion (S_e, P_e)

4. SUMMARY AND CONCLUSIONS

4.1 Summary

The numerical properties of implicit four-point difference schemes for the differential equations of unsteady flow have been analyzed. A summary of the results of the analytical analysis follows:

- 1 - A generalized expression, Eq. (18), for the stability factor $|\lambda|$ was developed using the von Neumann technique.
- 2 - When the finite difference weighting factor, θ , is within the interval $0.5 \leq \theta \leq 1.0$, the implicit four-point scheme is unconditionally linearly stable. When frictional effects are negligible, the box scheme, in which $\theta=0.5$, is neutrally or weakly stable; and, the backward implicit scheme, in which $\theta=1.0$, is unconditionally linearly stable independent of the computational time and distance steps.
- 3 - The truncation error, Eq. (27), of the implicit four-point scheme demonstrates the consistency of the scheme, since the truncation error approaches zero as the time and distance steps are refined.
- 4 - The truncation error indicates that the box scheme has second order accuracy; the accuracy decreases to the first order accuracy of the backward implicit scheme as θ increases from 0.5 to unity.
- 5 - Generalized convergence ratios for wave damping (C_d) and wave celerity (C) were developed; these are given by Eqs. (44) in terms of the following dimensionless parameters: (a) D_L , which is the ratio of the wave length to the computational distance step; (b) D_C , which is the Courant parameter given by Eq. (42b); (c) D_f , which is a dimensionless friction parameter given by Eq. (42c). Graphs of the convergence ratios plotted as functions of D_L , D_C , and D_f are presented in Figs. 2, 3, 4, and 5.
- 6 - As D_C increases, the convergence ratios tend to depart from a value of unity, i.e., the truncation error, which represents the departure of the difference solution from the true solution of the differential equation, increases as the Courant parameter increases. This trend may also be described for a given wave length by the following - the truncation error increases as the computational time step increases.
- 7 - As D_L increases, the convergence ratios tend to approach a value of unity, i.e., for a given wave length, the truncation error decreases as the computational distance step decreases.
- 8 - The convergence ratios tend to depart more from a value of unity as the friction parameter D_f increases, i.e., the truncation error increases as the frictional effects increase.
- 9 - The convergence properties of the box scheme are superior to those of the backward implicit scheme, particularly with respect to wave damping.
- 10 - The box scheme conserves mass during one time step.
- 11 - The box scheme conserves momentum during one time step if the equation of dynamic equilibrium is expressed in the form of Eq. (1b).

From the numerical simulation experiments, the following results are summarized:

- 1 - Numerical distortion, in the form of dispersion and damping of the computed transient, increases as the size of the Δt time step increases;
- 2 - Numerical distortion of the computed transient increases as the θ weighting factor in the implicit difference equations approaches unity;
- 3 - Numerical distortion, measured by S_e and P_e , is of the order of one percent or less for $\Delta t \leq 12$ hrs when the transients at the upstream boundary have a time of rise (τ) greater than approximately 72 hrs; this is applicable for $\theta=0.55$, $\bar{L}=100$ miles, and $\bar{n}=0.03$, and increases as θ , \bar{L} , and/or \bar{n} increase;
- 4 - When $\tau > 96$ hrs, the magnitude of the numerical distortion is approximately proportional to certain computational, upstream boundary, and channel parameters as follows:

$$[S_e, P_e] \propto \Delta t, \theta, \tau^{-1}, \rho, \bar{n}, \bar{L}, Y_o^{-1}, S_o^{-1}$$

- 5 - The implicit difference equations are more stable for large Δt time steps and relatively rapid transients ($24 \leq \tau \leq 48$ hrs) as θ approaches unity; however, the truncation error becomes quite large for Δt much greater than approximately 1 or 2 hrs.

4.2 Conclusions

From the results of the analytical and numerical simulation analyses of the numerical properties of the implicit four-point difference equations of unsteady flow, the following conclusions are presented:

- 1 - The numerical experiments tend to corroborate the results obtained via the analytical analysis of the linearized model equations of unsteady flow both as to the stability and convergence properties of the four-point implicit difference equations;
- 2 - The implicit four-point schemes with $0.5 \leq \theta \leq 1.0$ are unconditionally linearly stable; this is expected to always apply for long waves if the computational time and distance steps are selected to achieve a reasonable degree of convergence according to the criteria presented in Figs. 2-5;
- 3 - As θ departs from 0.5 and approaches 1.0, the accuracy of the implicit four-point schemes becomes less; therefore, the box scheme ($\theta=0.5$) is preferred over the backward implicit scheme ($\theta=1.0$), since the former has superior convergence properties;
- 4 - For the particular case of long duration smoothly varying transients of approximately eight days or greater, time steps in the range of 12 hrs ($D \approx 25$) may be used in the box scheme with negligible loss of accuracy; and
- 5 - The computational mode or pseudo-instability which is sometimes associated with the box scheme may be eliminated by increasing θ to a value of about 0.55.

REFERENCES

- Abbott, M. B., and Ionescu, F., "On the Numerical Computation of Nearly Horizontal Flows," J. Hydraul. Res., 5(2), 1967, pp. 97-117.
- Amein, M., "Streamflow Routing on Computer by Characteristics," Water Resour. Res., 2(1), 1966, pp. 123-130.
- Amein, M., and Fang, C. S., "Implicit Flood Routing in Natural Channels," J. Hydraul. Div. Amer. Soc. Civil Eng., 96(HY12), 1970, pp. 2481-2500.
- Baltzer, R. A., and Lai, C., "Computer Simulation of Unsteady Flows in Waterways," J. Hydraul. Div. Amer. Soc. Civil Eng., 94(HY4), 1968, pp. 1083-1117.
- Contractor, D. N., and Wiggert, J. M., "Numerical Studies of Unsteady Flow in the James River," VPI-WRRC-BULL 51, Water Resour. Res. Ctr., Va. Polytech. Inst. and State Univ., Blacksburg, Va., 1972.
- Dronkers, J. J., "Tidal Computations for Rivers, Coastal Areas, and Seas," J. Hydraul. Div. Amer. Soc. Civil Eng., 95(HY1), 1969, pp. 29-77.
- Fread, D. L., "Discussion of Implicit Flood Routing in Natural Channels," Amein and Fang, J. Hydraul. Div. Amer. Soc. Civil Eng., 97 (HY7), 1971,
- Fread, D. L., "Effects of Time Step Size in Implicit Dynamic Routing," Water Resour. Bull., 9(2), 1973a, pp. 338-351.
- Fread, D. L., "Technique for Implicit Dynamic Routing in Rivers with Tributaries," Water Resour. Res., 9(4), 1973b, pp. 918-926.
- Garrison, J. M., Granju, J. P., and Price, J. T., "Unsteady Flow Simulation in Rivers and Reservoirs," J. Hydraul. Div. Amer. Soc. Civil Engr., 95(HY5), 1969, pp. 1559-1576.
- Gunaratnam, D. J., and Perkins, F. E., "Numerical Solution of Unsteady Flows in Open Channels," Rep. 127, Hydrodyn. Lab., Dep. of Civil Eng., Mass. Inst. of Technol., Cambridge, Mass., 1970.
- Isaacson, E., and Keller, H. B., Analysis of Numerical Methods, John Wiley and Sons, New York, 1966.
- Lai, C., "Computation of Transient Flow in Rivers and Estuaries by the Multiple-reach Implicit Method," U.S. Geological Survey Prof. Paper 575-B, 1967, pp. B228-B232.
- Leendertse, J. J., "Aspects of a Computational Model for Long-Period Water-Wave Propagation," Rand Memorandum RM-5294-PR, Rand Corp., Santa Monica, Calif., 1967.
- Liggett, J. A., and Woolhiser, D. A., "Difference Solution of the Shallow-Water Equations," J. Eng. Mech. Div. Amer. Soc. Civil Eng., 95(EM2), 1967, pp. 39-71.
- Lister, M., "The Numerical Solution of Hyperbolic Partial Differential Equations by the Method of Characteristics," Math. Meth. for Dig. Comp., edited by A. Ralston and H. S. Wilf, Wiley & Sons, New York, 1960.
- O'Brien, G. G., Hyman, M. A., and Kaplan, S., "A Study of the Numerical Solution of Partial Differential Equations," J. Math. and Phys., 29(4), 1951, pp. 223-251.
- Stoker, J. J., Water Waves, Interscience Pub., New York, 1957.
- Strelkoff, T., "Numerical Solution of Saint-Venant Equations," J. Hydraul. Div. Amer. Soc. Civil Eng., 96(HY1), 1970, pp. 223-252.

(Continued from inside front cover)

- NWS HYDRO 13 Time Distribution of Precipitation in 4- to 10-Day Storms--Ohio River Basin. John F. Miller and Ralph H. Frederick, July 1972, 41 pp. (COM-72-11139)
- NWS HYDRO 14 National Weather Service River Forecast System Forecast Procedures. Staff, Hydrologic Research Laboratory, December 1972, 7 chapters plus appendixes A through I. (COM-73-10517)
- NWS HYDRO 15 Time Distribution of Precipitation in 4- to 10-Day Storms--Arkansas-Canadian River Basins. Ralph H. Frederick, June 1973, 45 pp. (COM-73-11169)
- NWS HYDRO 16 A Dynamic Model of Stage-Discharge Relations Affected by Changing Discharge. D. L. Fread, November 1973 (revised, October 1976), 38 pp. plus appendixes A and B. (COM-74-10818)
- NWS HYDRO 17 National Weather Service River Forecast System--Snow Accumulation and Ablation Model. Eric A. Anderson, November 1973.